Published online 10 February 2015 *Nucleic Acids Research, 2015, Vol. 43, No. 4* **2293–2312**
doi: 10.1093/nar/gkv028

Conformational changes in the P site and mRNA entry channel evoked by AUG recognition in yeast translation preinitiation complexes

Fan Zhang[1], Adesh K. Saini[1,2], Byung-Sik Shin[1], Jagpreet Nanda[3] and Alan G. Hinnebusch[1,*]

[1]Laboratory of Gene Regulation and Development, NICHD, NIH, Bethesda, MD 20892, USA, [2]Department of Biotechnology, Shoolini University of Biotechnology and Management Sciences, Solan, Himachal Pradesh-173212, India and [3]Laboratory on the Mechanism and Regulation of Protein Synthesis, NICHD, NIH, Bethesda, MD 20892, USA

Received September 25, 2014; Revised January 06, 2015; Accepted January 09, 2015

ABSTRACT

The translation preinitiation complex (PIC) is thought to assume an open conformation when scanning the mRNA leader, with AUG recognition evoking a closed conformation and more stable P site interaction of Met-tRNA$_i$; however, physical evidence is lacking that AUG recognition constrains interaction of mRNA with the 40S binding cleft. We compared patterns of hydroxyl radical cleavage of rRNA by Fe(II)-BABE tethered to unique sites in eIF1A in yeast PICs reconstituted with mRNA harboring an AUG or near-cognate (AUC) start codon. rRNA residues in the P site display reduced cleavage in AUG versus AUC PICs; and enhanced cleavage in the AUC complexes was diminished by mutations of scanning enhancer elements of eIF1A that increase near-cognate recognition *in vivo*. This suggests that accessibility of these rRNA residues is reduced by accommodation of Met-tRNA$_i$ in the P site (P_{IN} state) and by their interactions with the anticodon stem of Met-tRNA$_i$. Our cleavage data also provide evidence that AUG recognition evokes dissociation of eIF1 from its 40S binding site, ejection of the eIF1A-CTT from the P-site and rearrangement to a closed conformation of the entry channel with reduced mobility of mRNA.

INTRODUCTION

Identification of the translation initiation codon in eukaryotic mRNA typically occurs by a scanning mechanism whereby the 40S ribosomal subunit recruits initiator tRNA (Met-tRNA$_i$) in a ternary complex (TC) with eIF2-GTP, and the resulting 43S preinitiation complex (PIC) attaches to the mRNA 5′ end and scans the 5′UTR for complementarity with the anticodon of Met-tRNA$_i$ to identify the AUG start codon (1,2). The GTP in TC is hydrolyzed in the scanning complex, dependent on eIF5, but P_i release is blocked by eIF1, which also impedes stable binding of Met-tRNA$_i$ in the P site. AUG recognition triggers dissociation of eIF1 from the 40S subunit (3), which allows interaction between eIF5 and the C-terminal tail (CTT) of eIF1A (4), P_i release from eIF2-GDP·P_i (5) and more stable binding of TC that is thought to signify increased accommodation of Met-tRNA$_i$ in the P site (6) (Figure 1A). Subsequent dissociation of eIF2-GDP and other eIFs enables eIF5B-catalyzed subunit joining and formation of an 80S initiation complex with Met-tRNA$_i$ base paired to AUG in the P site (7).

It is believed that both eIF1 and scanning enhancer (SE) elements in the eIF1A CTT promote an open, scanning-conducive conformation of the PIC and the metastable mode of TC binding (the P_{OUT} state) that allows inspection of successive triplets entering the P site during the scanning process. A scanning inhibitor element (SI) in the eIF1A N-terminal tail (NTT) antagonizes SE function and promotes rearrangement to the closed state (8), with dissociation of eIF1 (9) and more stable TC binding in the P_{IN} conformation (10) (Figure 1A). X-ray crystal structures and cryo-EM models of various PICs (11–14) suggest that eIF1 physically obstructs Met-tRNA$_i$ binding in the P_{IN} state, thus favoring P_{OUT}, and the results of directed hydroxyl radical cleavage (DHRC) mapping of mammalian eIF1A suggested a similar role for the eIF1A CTT (15). Accordingly, accommodation of Met-tRNA$_i$ in the P_{IN} state should require displacement of both eIF1 and the eIF1A CTT from the immediate vicinity of the P site. By contrast, it appears that the eIF1A NTT interacts with the codon:anticodon duplex formed by base pairing of Met-tRNA$_i$ with AUG (14), consistent with its deduced function in promoting the P_{IN} state.

*To whom correspondence should be addressed. Tel: +301 496 4480; Email: ahinnebusch@nih.gov

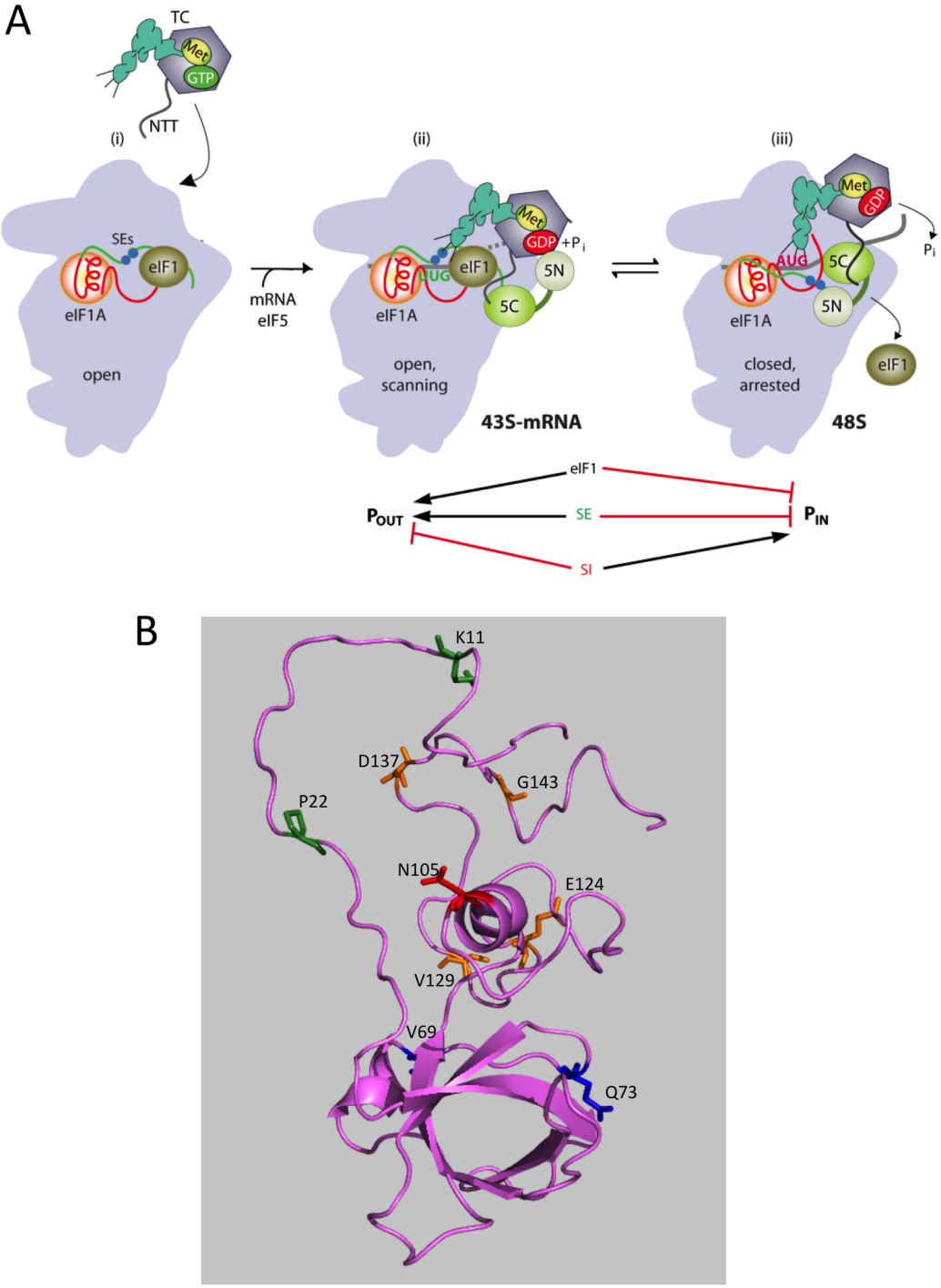

Figure 1. Model describing conformational rearrangements of the PIC during scanning and start codon recognition and locations of cysteine substitutions in eIF1A employed for DHRC mapping. (**A**) eIF1 and the scanning enhancer (SE) elements in the CTT of eIF1A stabilize an open conformation of the 40S subunit to which the TC loads rapidly. (ii) The 43S PIC in the open conformation scans the mRNA for the start codon with Met-tRNA$_i$ bound in the P$_{OUT}$ state. The GAP domain in the N-terminal domain of eIF5 (5N) stimulates GTP hydrolysis by the TC to produce GDP•P$_i$, but release of P$_i$ is blocked. The unstructured NTT of eIF2β interacts with eIF1 to stabilize eIF1•40S association and the open conformation. (iii) On AUG recognition, Met-tRNA$_i$ moves from the P$_{OUT}$ to P$_{IN}$ state, clashing with eIF1 and the CTT of eIF1A. Movement of eIF1 and the eIF1A CTT away from the P site disrupts eIF1′s interaction with eIF2β-NTT, and the latter interacts with the eIF5-CTD instead. eIF1 dissociates from the 40S subunit, and the eIF5-NTD disengages from eIF2 and interacts with the eIF1A CTT instead, dependent on the SE elements, thereby facilitating P$_i$ release from eIF2. The eIF5-CTD moves into the position on the 40S subunit previously occupied by eIF1 and blocks re-association of eIF1. (Below) Arrows summarize that eIF1 and the eIF1A SE elements promote P$_{OUT}$ and block transition to the P$_{IN}$ state, whereas the scanning inhibitor (SI) element in the NTT of eIF1A stabilizes the P$_{IN}$ state. (Adapted from (4,33)). (**B**) Cartoon depiction of a model of yeast eIF1A created with I-TASSER (http://zhanglab.ccmb.med.umich.edu/I-TASSER) using as template the solution structure of human eIF1A (34) (pdb: 1D7Q). The predicted structure is shown in 'ribbons' depiction using PyMOL (35), with side chains of residues substituted with cysteine in single-Cys variants depicted as sticks and colored according to location in eIF1A: NTT (green), OB-fold (blue), helical domain (red) and CTT (gold).

Genetic experiments have implicated eIFs 1, 1A, 5 and 2 in accurate AUG selection in living cells. Sui$^-$ (Suppressor of initiation codon) mutations in these factors allow increased initiation at near-cognate triplets, like UUG or AUC (10,16–17). Sui$^-$ mutations in the eIF1A SE elements appear to destabilize the open/P_{OUT} conformation, enhancing transition from the open/P_{OUT} to closed/P_{IN} state at near cognates; and they also reduce the rate of TC loading (10), as TC binds most rapidly to the open conformation (6). The effects of SE mutations are complex, however, as they additionally disfavor P_i release from eIF2 following dissociation of eIF1 at AUG codons, most likely by impeding interaction between the eIF1A CTT and the eIF5-NTD that is evoked by AUG recognition (4). Thus, the eIF1A CTT has a dual function of stabilizing P_{OUT} and blocking rearrangement to P_{IN} at near cognates in the open complex, while enabling P_i release following eIF1 dissociation in the closed/P_{IN} complex on AUG recognition.

Recent structural analysis of reconstituted yeast or mammalian PICs supports the notion of a conformational rearrangement of the PIC on start codon recognition. Comparisons of X-ray crystal structures of mammalian 40S complexes harboring eIF1, eIF1+eIF1A or eIF1A+mRNA+$tRNA_i$ with $tRNA_i$ base paired to AUG (partial mammalian 48S (pm48S) complex) suggested that Met-$tRNA_i$ is bound to the P site in the scanning complex in a manner that avoids steric clash with eIF1, and becomes more locked into the P-site on AUG recognition. In the 40S·eIF1 and 40S·eIF1·eIF1A complexes, the location of P-site 18S rRNA residues would allow Met-$tRNA_i$ to tilt toward the E-site and avoid a clash with eIF1, fulfilling the requirements of the P_{OUT} state. In the pm48S complex, by contrast, helix 29 (h29) is displaced toward the A-site and, together with h24, prevents tilting of Met-$tRNA_i$ toward the E-site to stabilize a 'P/I-like' state that clashes with eIF1, as predicted for the P_{IN} state (13). A more recent cryo-EM model of a partial yeast 48S (py48S) complex containing eIF1A+eIF1+mRNA+TC with Met-$tRNA_i$ base paired with AUG showed a P/I state (eP/I') more similar to the hybrid P/E state seen during translocation in the elongation stage of protein synthesis (14). It also resembles the eP/I" conformation observed in the cryo-EM model of a mammalian 43S PIC containing eIFs 1, 1A, 3, TC and helicase Dhx29 (but lacking mRNA; the pm43S complex) with the important distinction that the anticodon stem-loop (ASL) is ∼7Å deeper in the P site in the yp48S versus the pm43S complex, presumably reflecting the P_{OUT} to P_{IN} transition evoked by AUG recognition.

Previous cryo-EM analysis of a yeast 40S·eIF1·eIF1A complex suggested that eIF1 and eIF1A provoke a structural rearrangement of the yeast 40S that involves an open conformation of the 'latch' of the mRNA entry channel, envisioned to be conducive to scanning. The latch is formed by non-covalent interactions between residues of h18 in the body of the 40S subunit and h34 in the 40S head domain. By contrast, a yeast 40S·eIF1A complex, which could mimic the PIC following eIF1 release at the start codon, displayed a closed-latch conformation regarded as incompatible with scanning. However, the mRNA entry channel latch is apparently closed in the mammalian (13) and *Tetrahymena* (12) 40S·eIF1·eIF1A crystal structures; and it was proposed that latch closure in the scanning PIC serves to lock mRNA into the 40S mRNA-binding cleft and increase the processivity of scanning, whereas the open-latch conformation seen in the yeast 40S·eIF1·eIF1A complex would enable initial attachment of the 43S PIC to mRNA (13). A more recent, higher resolution cryo-EM structure of the yeast 40S·eIF1·eIF1A complex also exhibits a closed-latch conformation (14), making it unclear whether the transition from the open/P_{OUT} to closed/P_{IN} state entails closure of the latch or changes in the dimensions of the mRNA entry channel.

As mentioned above, there is evidence that the eIF1A CTT functions together with eIF1 to promote the open/P_{OUT} state of the PIC and also must be displaced together with eIF1 from near the P site to allow stable binding of Met-$tRNA_i$ in the P_{IN} state of the closed complex (10,15). We set out to test this hypothesis by attempting to detect distinct locations of the CTT in yeast PICs reconstituted with mRNAs either containing or lacking an AUG codon by conducting DHRC of 18S rRNA by eIF1A proteins derivatized with Fe(II)-BABE at unique surface-exposed cysteines in the CTT. The results of our experiments support the idea that the CTT is displaced from the P site in the closed/P_{IN} state. In addition, analysis of cleavage patterns produced by eIF1A derivatives with single-Cys residues in the NTT or oligonucleotide-binding (OB)-fold provide evidence for a conformational change triggered by AUG recognition that involves more extensive interaction of Met-$tRNA_i$ with the P site, likely reflecting the P_{OUT} to P_{IN} transition, and the dissociation of eIF1 from the 40S platform. The results also suggest that AUG recognition evokes a narrowed conformation of the mRNA entry channel, or constrained interaction of mRNA with this portion of the mRNA binding cleft, plus a more closed conformation of the entry channel latch.

MATERIALS AND METHODS

Plasmid and yeast strain constructions

Plasmids used in this study are listed in Table 1.*TIF11* mutant alleles were constructed by fusion PCR using p3390, pAS22 or pA72 containing *TIF11* mutant alleles, as template, as described previously (18,10,19). The fusion PCR products were inserted between the *EcoR* I and *Sal* I sites of YCplac111 (sc) or YCplac181 (hc), and the subcloned fragments of all mutant constructs were confirmed by DNA sequencing (20). Yeast strain H3582 was described previously (21). Plasmids used to express intein-eIF1A proteins in *Escherichia coli* were made by PCR amplification of the appropriate DNA fragments from WT or mutant *TIF11* templates with insertion of the resulting fragments into expression vector pTYB2 (New England BioLabs).

Biochemical assays in the reconstituted *in vitro* system

Reagent preparation. Initiation factors eIF5, eIF1 and eIF1A (WT and mutant variants) were purified using the IMPACT system (New England BioLabs) as previously described (22). His-tagged eIF2 was overexpressed in yeast and purified as described (22). 40S subunits were purified as described previously (22). The sequences of the model

Table 1. Plasmids used in this study

Plasmid	Description	Source or reference
YCplac111	sc *LEU2* vector	(20)
P3390	sc *LEU2 TIF11* in YCplac111	(18)
pAS22	sc *LEU2 tif11-SE** in YCplac111	(10)
pAS72	sc *LEU2 tif11-C51S-C89S* in YCplac111	(19)
pAS73	sc *LEU2 tif11-SE*-C51S-C89S* in YCplac111	This study
pAS74	sc *LEU2 tif11-C51S-C89S-K11C* in YCplac111	This study
pAS86	sc *LEU2 tif11-SE*-C51S-C89S-K11C* in YCplac111	
pAS75	sc *LEU2 tif11-C51S-C89S-P22C* in YCplac111	This study
pAS78	sc *LEU2 tif11-C51S-C89S-V69C* in YCplac111	This study
pAS79	sc *LEU2 tif11-C51S-C89S-Q73C* in YCplac111	This study
pAS80	sc *LEU2 tif11-C51S-C89S-N105C* in YCplac111	This study
pAS81	sc *LEU2 tif11-C51S-C89S-E124C* in YCplac111	This study
pAS82	sc *LEU2 tif11-C51S-C89S-V129C* in YCplac111	This study
pAS87	sc *LEU2 tif11-SE*-C51S-C89S-V129C* in YCplac111	This study
pAS83	sc *LEU2 tif11-C51S-C89S-D137C* in YCplac111	This study
pAS84	sc *LEU2 tif11-C51S-C89S-G143C* in YCplac111	This study
pTYB2	IMPACT vector	New England Biolabs
pAS96	*tif11-C51S-C89S* in pTYB2	This study
pLfz515–1	*tif11-C51S-C89S-K11C* in pTYB2	This study
pLfz521R-6	*tif11-SE*-C51S-C89S-K11C* in pTYB2	This study
pAS98	*tif11-C51S-C89S-P22C* in pTYB2	This study
pAS100	*tif11-C51S-C89S-V69C* in pTYB2	This study
pAS101	*tif11-C51S-C89S-Q73C* in pTYB2	This study
pAS102	*tif11-C51S-C89S-N105C* in pTYB2	This study
pLfz516–2	*tif11-C51S-C89S-A113C* in pTYB2	This study
pAS103	*tif11-C51S-C89S-E124C* in pTYB2	This study
pLfz552–9	*tif11-C51S-C89S-V129C* in pTYB2	This study
pLfz554–2	*tif11-SE*-C51S-C89S-V129C* in pTYB2	This study
pAS106	*tif11-C51S-C89S-D137C* in pTYB2	This study
pLfz553–5	*tif11-C51S-C89S-G143C* in pTYB2	This study

mRNAs were 5′-GGAA[UC]$_7$UAUG[CU]$_{10}$C-3′ and 5′-GGAA[UC]$_7$UUUG[CU]$_{10}$C-3′. Yeast tRNA$_i^{Met}$ was synthesized from a hammerhead fusion template using T7 polymerase transcription and charged with [^{35}S]-Met or unlabeled methionine as previously described (22). Cys-less eIF1A and its single-Cys variants were derivatized with Fe(II)BABE essentially as described (23).

43S·mRNA PICs formation assay. Gel shift assays were performed to analyze the 43S·mRNA PIC formation as described previously (24). 43S·mRNA(AUG) complexes were assembled using purified 40S ribosomal subunits (0.4 μM), eIF1 (0.8 μM), eIF5 (0.8 μM), pre-formed TC (containing purified eIF2 (0.8 μM), [^{35}S]-Met-tRNA$_i$ (0.5 nM) and saturating GDPNP (1 mM)), mRNA(AUG) (1 μM) and the indicated BABE-derivatized eIF1A variants (0.8 μM). The reactions were stopped with addition of 2 μl of native gel dye (50% sucrose, 0.02% Bromophenol Blue, 0.02% Xylene Cyanol) and immediately followed by loading onto a running native gel. 43S·mRNA(AUC) complexes were assembled similarly except they contained mRNA(AUC) at the same (1X) or 10-fold higher (10X) concentration of that used for mRNA(AUG).

Hydroxyl radical cleavage. For hydroxyl radical cleavage of 18S rRNA, 0.8 μM Fe(II)BABE-eIF1A variants were used to make 43S·mRNA PICs by assembling 0.4 μM 40S ribosomes, pre-formed TC (0.8 μM eIF2, 0.8 μM Met-tRNA$_i$, 1 mM GDPNP), 0.8 μM eIF1 and 0.8 μM eIF5 in the presence or absence of 1 μM mRNA(AUG or AUC). Briefly, 40S ribosomes, eIF1 and eIF5 were mixed together and added to Fe(II)BABE-eIF1A variants, and the reaction mixture was kept on ice. TC was pre-formed by incubating eIF2 and GDPNP at 26°C for 10 min and then adding Met-tRNA$_i$ and incubating for 5 min at 26°C. Pre-formed TC was combined with the pre-assembled 40S·eIF1·Fe(II)BABE-eIF1A·eIF5·mRNA(AUG or AUC) complexes and the final PIC mixture was incubated at 30°C for 30 min and then on ice for 10 min. To each 20 μl of PIC mixture, 1 μl ascorbic acid (100 mM) was added and kept for 15 s at (26°C), after which 1 μl of H_2O_2 (0.5%) was added and incubated for 15 s at (26°C). After incubation on ice for 10 min, 2 μl 100 mM thiourea was added to quench the cleavage reactions. RNA extraction was conducted using Qiagen RNeasy kit. Cleavage sites on 18S rRNA were detected by primer extension using reverse transcriptase and oligonucleotide primers as described previously (23,25).

RESULTS

Unique cysteine substitutions in eIF1A have little or no effect on eIF1A function *in vivo* or *in vitro*

The initial goal of our study was to detect a conformational change in the eIF1A CTT in the 43S·mRNA PIC on recognition of an AUG start codon, involving an adjustment of the CTT's location in the P site to accommodate the P$_{IN}$ state of Met-tRNA$_i$. To this end, we carried out DHRC of 18S rRNA by eIF1A proteins derivatized with Fe(II)-BABE at unique surface-exposed cysteines located in the CTT or, as controls, in the NTT or globular domain of the protein. We began by conducting site-directed mutagenesis of the plasmid-borne *TIF11* gene, en-

coding yeast eIF1A, to substitute the two naturally occurring Cys residues (Cys-51 and Cys-89) with Ser ('Cys-less' eIF1A), and then made single-Cys substitutions at nine different positions in eIF1A, including locations in the NTT (K11C, P22C), OB-fold (V69C and Q73C), helical domain (N105C) and CTT (E124C, V129C, D137C, G143C) (Figure 1B and Supplementary Figure S1). We also generated mutant versions of K11C and V129C harboring Ala substitutions of the scanning enhancer elements (SE_1 and SE_2) in the CTT (referred to here as the SE* substitutions) (10). The resulting alleles were tested for the ability to replace WT *TIF11* as the only source of eIF1A in a *tif11Δ* yeast strain (lacking chromosomal *TIF11*) by plasmid shuffling (26). All nine single-Cys mutant alleles could substitute for WT *TIF11* and support cell growth on complete (YPD) medium at a level that was essentially indistinguishable from WT for seven of the nine alleles, and somewhat reduced from WT in the case of *K11C* and *N105C* (Supplementary Figure S2). The *SE** mutation is lethal (10), which was also found to be the case for the *K11C,SE** and *V129C,SE** alleles.

Subsequently, the WT and single-Cys eIF1A derivatives were expressed in bacteria, purified and derivatized with Fe(II)-BABE, and the derivatized proteins were used to reconstitute PICs containing 40S subunits, eIF1, eIF1A, TC (assembled with nonhydrolyzable GDPNP), eIF5 and either (i) no mRNA; (ii) a synthetic model mRNA containing a near-cognate AUC start codon [mRNA(AUC)]; or an otherwise identical mRNA with an AUG codon [mRNA(AUG)]. In reconstituting these PICs, 40S subunits were present at 0.4 μM, whereas all other components were present at 2- to 3-fold higher concentrations (or 20-fold higher for some experiments with mRNA(AUC)), which all correspond to saturating concentrations for PIC assembly (22). We verified that all of the Fe(II)-BABE derivatives were able to form 43S·mRNA(AUG) complexes using an assay that detects a mobility shift in native gel electrophoresis of [^{35}S]-methionine-labeled TC on stable binding to the 40S subunit (22). The endpoints of the reactions were indistinguishable from that achieved with WT eIF1A for all single-Cys variants except K11C and the two SE* derivatives, which showed slight or moderately reduced amounts of 43S·mRNA complexes, respectively, in this assay (Supplementary Figure S3; see also AUG complexes in Supplementary Figure S4A and B).

Previously, we showed that the SE* substitutions increase the K_d for TC binding to 43S·mRNA(AUG) complexes from ≤0.5 nM to ∼4 nM (10); however, because 40S subunits were employed here at a concentration that is ∼100-fold higher than the K_d determined for the eIF1A SE* variant, the diminished endpoint observed for the SE* variants with mRNA(AUG) is unlikely to result from a failure to drive PIC assembly to completion. We concluded previously that the endpoints of TC binding reactions at high concentrations of 40S subunits reflect the distribution of PICs in the open versus closed states. The open state was proposed to be unstable during electrophoresis, leading to endpoints of <1 (measured as fractions of TC bound to 40S complexes) in situations where open complex persists, such as with 43S PICS (no mRNA) or 43S·mRNA PICs assembled with mRNAs containing a near-cognate start codon (27,28). This interpretation was supported by the reduced endpoints observed in forming 43S·mRNA(AUG) complexes with $tRNA_i$ mutants that destabilize P_{IN} and favor P_{OUT} (29). Hence, the reduced endpoints observed here for the SE* variants at saturating concentrations of 40S subunits most likely reflect the reduced occupancy of the P_{IN} state, leading to dissociation of a fraction of the 43S·mRNA(AUG) complexes during gel electrophoresis, rather than a diminished capacity to form 43S·mRNA(AUG) complexes in solution. Supporting this interpretation, we consistently observed a smear of Met-$tRNA_i$ in the lanes for the K11C/SE* and V129C/SE* variants in assays of 43S·mRNA(AUG) assembly (Supplementary Figure S3), likely representing dissociation from the PICs and subsequent accelerated migration of unbound Met-$tRNA_i$ during electrophoresis. Moreover, reduced endpoints and apparent dissociation of Met-$tRNA_i$ during electrophoresis was also observed for WT and all eIF1A variants in PICs formed with mRNA(AUC), and this outcome was largely unaffected by increasing the mRNA concentration from 1 μM to 10 μM (Supplementary Figure S4A and B). (The reduced endpoint for the mRNA(AUG) complex with WT eIF1A in the left panel of Supplementary Figure S4B was not observed in any replicate experiments, including those in Supplementary Figures S3 and S4A and the right panel of S4B.) Hence, we consider it likely that all of the eIF1A variants assemble complexes in solution at levels similar to that given by WT eIF1A, for both mRNA(AUG) and mRNA(AUC), with the differences among variants and mRNAs limited to the partitioning of complexes between the open/P_{OUT} and closed/P_{IN} states.

Fe(II)-BABE tethered to unique sites in eIF1A directs hydroxyl radical cleavage of residues in the decoding center of reconstituted yeast PICs

By comparing the cleavage patterns produced by single-Cys derivatives to those given by Cys-less eIF1A, we identified specific cleavages of 18S rRNA that were dependent on the presence of the unique Cys residue for all 11 derivatives. As described below, all cleavages involve residues located in the decoding center or mRNA entry channel of the 40S subunit, which is consistent with the location of eIF1A near the A site deduced from DHRC-mapping of eIF1A in reconstituted mammalian PICs (15), and revealed in crystal structures of 40S·eIF1·eIF1A PICs from *Tetrahymena* (12) and mammals (13), and in cryo-EM models of the yeast 40S·eIF1·eIF1A and yp48S complexes (14). For reference purposes, Supplementary Table S1 contains a summary of all rRNA residues cleaved specifically by each of the single-Cys derivatives and indicates whether cleavage intensity was relatively suppressed or enhanced in 43S·mRNA(AUG) versus 43S·mRNA(AUC) PICs. The locations of the corresponding rRNA residues in the cryo-EM model of the yp48S complex (14) are depicted in Figure 2 and Supplementary Figure S5. The locations of the Cys residues are also indicated there, except for those in the CTT whose positions in the structure are unknown. The remainder of this section presents an overview of the cleavage patterns observed for different eIF1A variants as a prelude to describing the cleavage data and the influence of an AUG start codon on cleavage intensities.

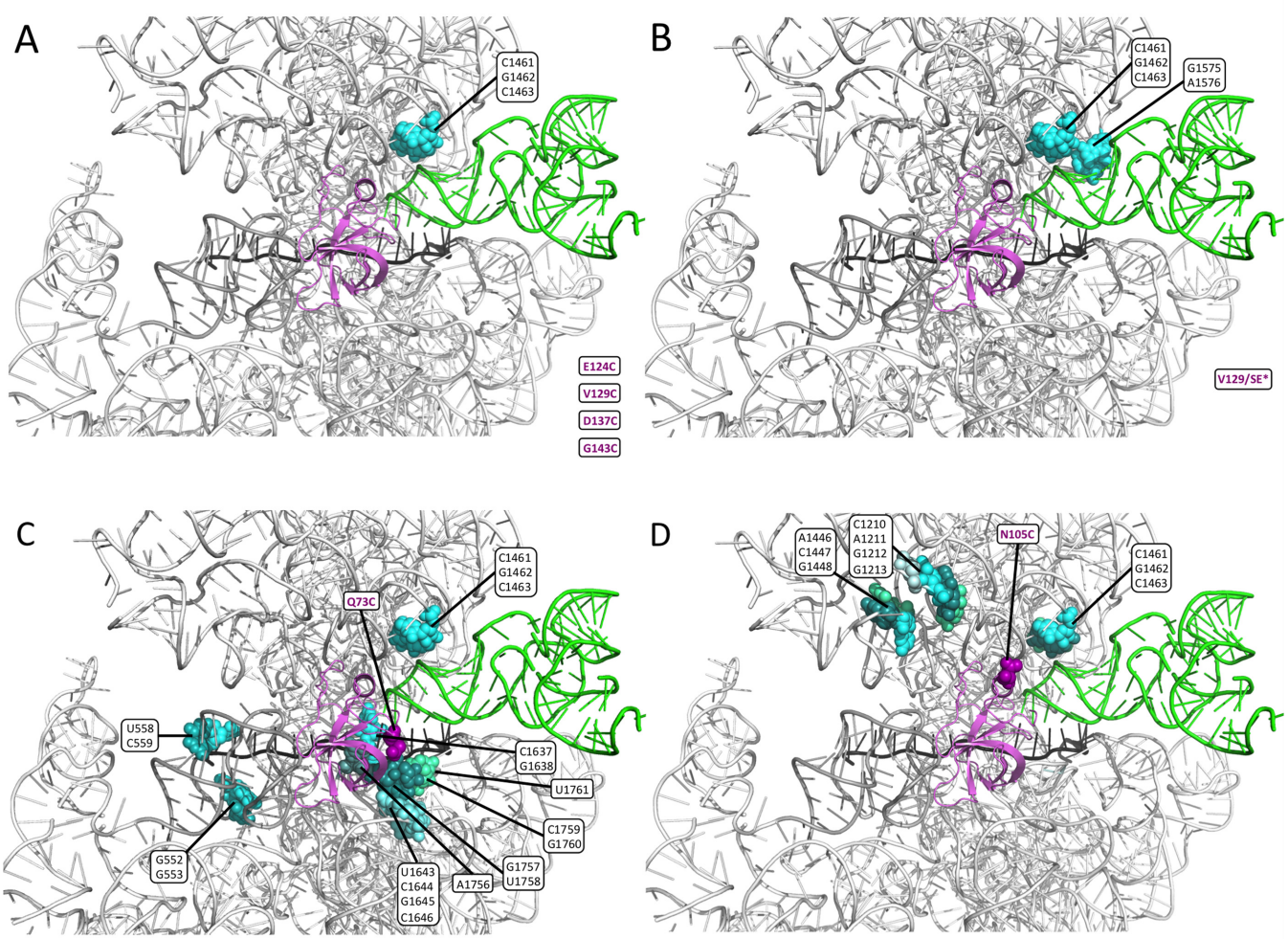

Figure 2. Summary of 18S rRNA residues cleaved by single-Cys variants. (**A–D**) 18S rRNA residues cleaved by the eIF1A single-Cys variants, labeled with magenta lettering, are depicted as spheres in different shades of blue or green (chosen only to distinguish adjacent residues belonging to a single cluster) in the yp48S complex containing eIF1, eIF1A, mRNA(with an AUG) and TC (14). A cartoon of this PIC created with PyMOL displays eIF1A (magenta), $tRNA_i$ (green), mRNA (black) and the 18S rRNA in either white or gray (for helices in the decoding center: 18, 28, 29, 30, 31, 34 and 44). All ribosomal proteins are hidden. The locations in eIF1A of the single-Cys residues in the different variants are depicted with magenta spheres, except for CTT residues E124C, V129C, D137C and G143C (A–B), which were not resolved in that PIC structure.

The derivatives with single-Cys substitutions in the CTT produced many fewer cleavages compared to the derivatives with Cys residues in the NTT or OB-fold. In fact, the CTT single-Cys variants, including E124C (within SE_1), V129C (between SE_1 and SE_2), D137C (within SE_2) and G143C (C-terminal to SE_2), produced significant, reproducible cleavages of only three 18S rRNA residues, C1461/G1462/C1463. Interestingly, these consecutive rRNA residues are located in h30 in proximity to the ASL of $tRNA_i$ in the py48S PIC (14) (Figure 2A, cyan spheres). In addition to these three cleavages in h30, the SE* mutant derivative of the CTT variant V129C (V129C/SE*) also produced strong cleavage of P-site residues G1575 and A1576 found in the loop between h29 and h42 (Figure 2B). While these cleavages of P-site residues are consistent with the predicted location of the CTT in the P-site (15), all of the Cys-substituted derivatives we examined directed cleavage of the three h30 residues (C1461/G1462/C1463), and cleavage of G1575 and A1576 was also conferred by V69C (in the OB-fold domain) and by K11C and P22C in the NTT (Figure 2 and Supplementary Figure S5). Thus, we assume that these rRNA residues are susceptible to cleavage by hydroxyl radicals generated from diverse locations within eIF1A, which can follow an unobstructed path to the P-site in the reconstituted PICs.

In addition to the ubiquitously cleaved h30 residues, the Q73C and N105C variants each conferred strong cleavage of additional residues, which differed for these two variants in a manner consistent with their locations in eIF1A. As summarized in Figure 2C, residue Q73C (depicted in eIF1A as magenta spheres) evoked cleavage of 12 residues at the top of h44, which is in proximity to this segment of the eIF1A OB-fold encompassing Q73C, and four residues in h18. By contrast, helical domain residue N105C conferred cleavage of residues in h32 or in the loop between h32 and h34, which are close to one another in the head domain of the 40S subunit and near the helical region of eIF1A (Figure 2D).

The OB-fold variant V69C conferred many more cleavages than did Q73C, including additional residues in the P-site and numerous residues in h34 or h18 located in the mRNA entry channel (Supplementary Figure S5A). Despite the dispersed nature of these cleavages, they are clearly centered on the position of V69C in eIF1A. The much greater number of cleavages produced by V69C versus Q73C might be explained by the fact that V69 is located on the face of the OB-fold that points inward to the 40S subunit, whereas Q73 is on the surface facing outward to the solvent (Supplementary Figure S5A versus Figure 2C) (12–14). Both NTT variants K11C and P22C, and the SE* derivative of K11C, also generated relatively large numbers of cleavages that overlapped extensively with those given by V69C (Supplementary Figure S5A–C). This extensive overlap is consistent with the fact that these NTT residues, like V69, reside in proximity to the decoding center in the interior of the 40S subunit (14). As discussed next, many of the cleavages shared between these two NTT Cys residues and V69C display greater cleavage in PICs reconstituted with mRNA(AUC) versus mRNA(AUG), indicating conformational differences between these two complexes.

Evidence for rearrangement to a closed conformation of the P site and rRNA–tRNA$_i$ interactions on AUG recognition

P site residues G1575–A1576–A1577–U1578. In an effort to detect rearrangements in the 40S decoding center evoked by AUG recognition, we initially compared the pattern of cleavages directed by particular Cys residues in PICs reconstituted either without mRNA or with mRNA(AUG). As noted above, the P site residues G1575/A1576 were cleaved by several single-Cys variants (Figure 2B and Supplementary Figure S5A–C). Interestingly, these rRNA residues are poised to make A-minor interactions with the invariant G:C base pairs of the tRNA$_i$ ASL (Figure 2B) (13), and genetic evidence suggests that both G1575/A1576 and the ASL G:C base pairs contribute to start codon recognition in yeast cells (30,31). As shown in Figure 3A, we observed more intense cleavage of these two residues, along with adjacent residues A1577–U1578, in the No-mRNA versus mRNA(AUG) complexes for several single-Cys variants. This distinction was most pronounced for the K11C, P22C and V69C variants that, together with V129C/SE*, also showed the most intense cleavage of this set of four residues in the No-mRNA complex among all of the eIF1A variants tested. The differential cleavage between No-mRNA and mRNA(AUG) complexes observed for the K11C, P22C and V69C variants is designated by using blue labels for these three single-Cys derivatives and blue dots inserted to the left of the relevant bands in the mRNA(AUG) lanes of the gel in Figure 3A. The locations of the cleaved residues are indicated with black dots in the secondary structure depiction of the relevant portion of the secondary structure map of 18S rRNA in Figure 3C.

To determine whether the aforementioned differential cleavage of residues 1575–1578 merely reflects the absence or presence of mRNA or, rather, a conformational change in the PIC provoked by AUG recognition, we compared the mRNA(AUG) complexes to both mRNA(AUC) and No-mRNA complexes in subsequent experiments. As shown in Figure 3B and Supplementary Figure S6, the P22C and V69C variants displayed relatively greater cleavage of G1575–U1578 in the mRNA(AUC) versus mRNA(AUG) complexes, but similar cleavage intensities in the mRNA(AUC) and No-mRNA complexes. This differential cleavage was also obvious at residues A1577–U1578 for the K11C variant (Figure 3B and Supplementary Figure S6). Quantification of band intensities from replicate experiments indicated a diminished mean cleavage intensity of residue A1576 in the AUG versus AUC complexes for K11C (Figure 3D), although the differential cleavage was less pronounced than that given by V69C for both this residue and G1575 (Figure 3B and D). This pattern of differential cleavage is dubbed 'AUC>AUG cleavage' and is summarized for the relevant residues by highlighting them in blue in the yp48S PIC depicted in Figure 4. (As done here for results presented in Figure 3B and Supplementary Figure S6, below we present data from replicate experiments in the supplementary figures for reference purposes only. Quantification of band intensities from replicate experiments was conducted to confirm differential cleavage between AUG and AUC/No-mRNA complexes when this outcome was not obvious from visual inspection of replicate gel data, which invariably was limited to certain cleavages obtained with K11C.)

The fact that cleavage of G1575–U1578 directed by Cys residues located in either the NTT (K11C, P22C) or OB-fold (V69C) is suppressed in the AUG complex seems most consistent with the idea that AUG recognition promotes a conformational change that reduces the susceptibility of these rRNA residues to hydroxyl radical cleavage, rather than altering the locations of the derivatized Cys residues in a way that moves all three of them farther from the P site. Considering the proximity of G1575–U1578 to the tRNA$_i$ ASL (Figure 4), we thus propose that PIC rearrangement from the P$_{OUT}$ state (at AUC) to P$_{IN}$ state (at AUG) alters Met-tRNA$_i$ binding in the P site in a manner that reduces susceptibility of these rRNA residues to hydroxyl radical cleavage directed by K11C, P22C and V69C.

Consistent with this proposal, the presence of SE* substitutions in the K11C variant nearly eliminated cleavage of A1577 and U1578 by the K11C/SE* variant in the AUC and No-mRNA complexes (Figure 3B and Supplementary Figure S6). Because K11C (with WT SE elements) confers no cleavage of these two residues above background levels in the AUG complex, the SE* substitutions reduce cleavage of A1577–U1578 by K11C specifically in the AUC and No-mRNA PICs, such that cleavage occurs only slightly above background in all three complexes. To summarize the finding in the PIC structure of Figure 4 that the SE* substitutions diminish the AUC>AUG cleavage of A1577–U1578 in the K11C/SE* variant by suppressing cleavage in the AUC complex, these two residues are depicted with side chains in 'stick' representation as well as blue color. This suppression of A1577–U1578 cleavage in the AUC complex suggests that the P$_{IN}$ conformation of Met-tRNA$_i$ binding is enhanced at AUC codons by the SE* substitutions in K11C in the same manner observed at AUG codons for the K11C variant with WT SE elements, which seems consistent with the increased frequency of initiation at near-cognate

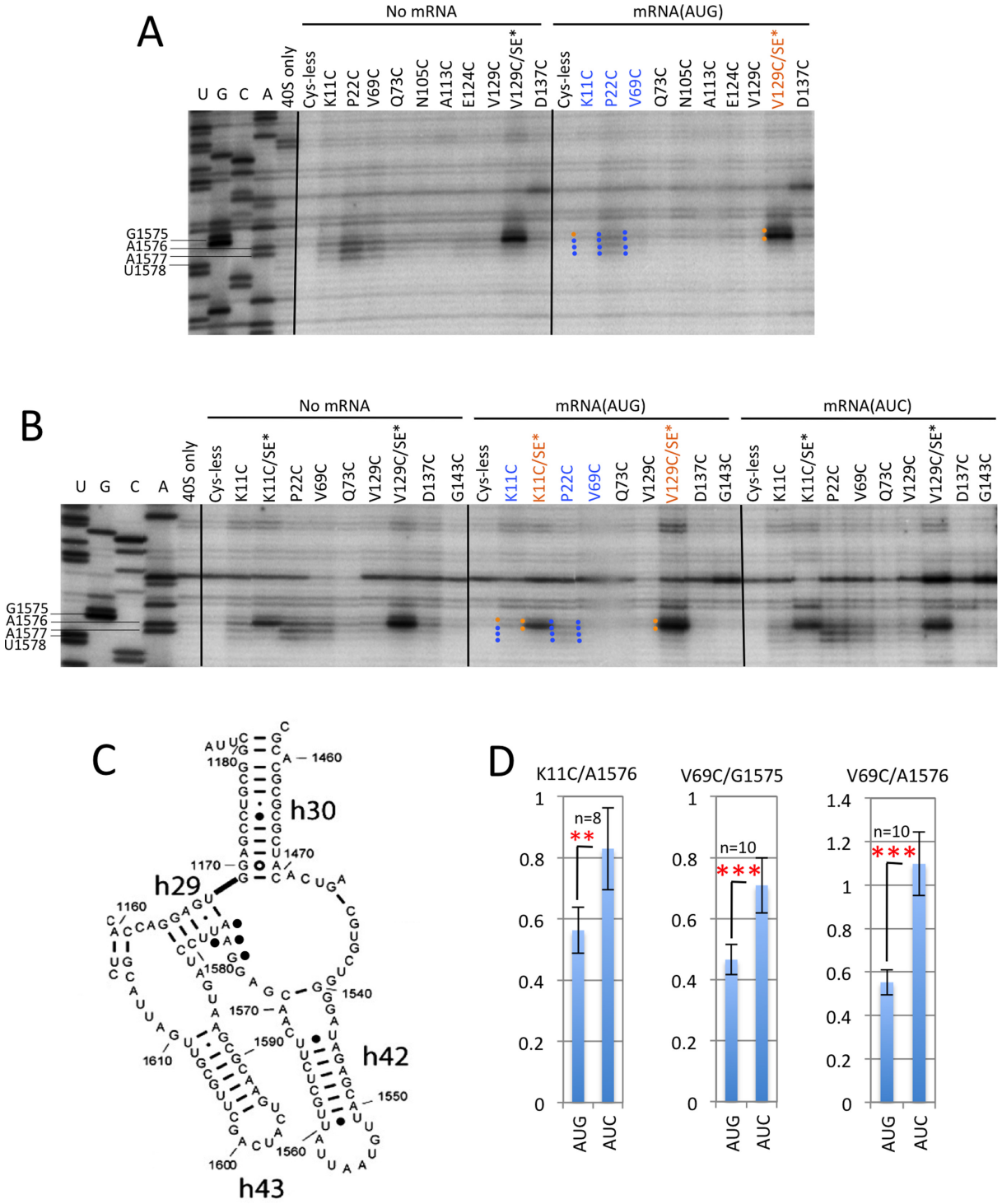

Figure 3. DHRC of P-site residues within or proximal to h29 by eIF1A variants K11C, P22C and V69C is modulated by start codon recognition in reconstituted PICs. (**A–B**) Sites of cleavage of 18S rRNA by hydroxyl radicals directed from Fe(II)BABE tethered to unique cysteines in eIF1A single-Cys variants in 43S PICs (No-mRNA) or 43S·mRNA PICs assembled with either mRNA(AUG) or mRNA(AUC) mapped by primer extension inhibition. Lanes U, G, C, A depict the relevant portion of the yeast 18S rRNA sequence ladder generated using the same primer, and locations and sequences of cleaved residues are indicated in the ladder. Blue dots to the left of the relevant bands indicate cleavages that are more intense in the No-mRNA or mRNA(AUC) complexes compared to the mRNA(AUG) complex directed by the relevant eIF1A variant for that lane, whereas gold dots signify constitutive cleavage in all three complexes. Labels of the variants listed at the top are similarly color-coded. (**C**) A portion of the yeast 18S rRNA secondary structure reproduced from (36) with black dots inserted adjacent to the cleaved residues under consideration. (**D**) Cleavage of the indicated residues by the K11C or V69C derivatives was quantified in replicate experiments by phosphorimaging analysis of the intensity of the relevant band, relative to a nearby reference band exhibiting constitutive cleavage for all eIF1A derivatives, for the AUG and AUC complexes examined on the same gel. The paired normalized intensities for the AUG and AUC complexes were subjected to a Student's paired *t* test for the indicated number of replicate gels (*n*) with the resulting *P* values indicated as ≤0.05 (*), ≤0.01 (**), ≤0.001 (***).

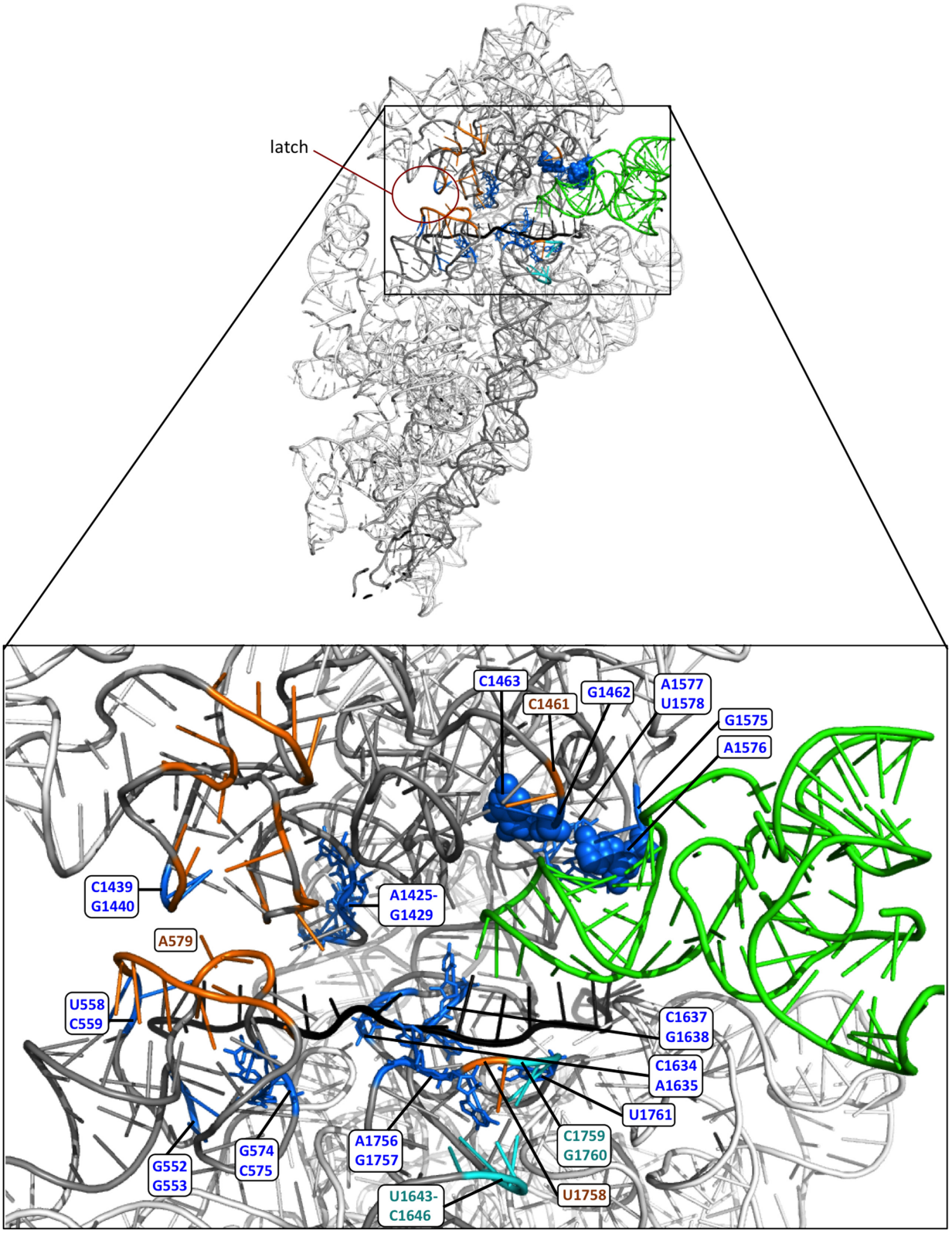

Figure 4. Summary of the influence of AUG recognition on cleavage of 18S rRNA residues in the PIC. The locations of 18S rRNA cleavages are depicted in the yp48S PIC (14), with $tRNA_i$, mRNA and 18S rRNA colored as in Figure 2. 18S rRNA residues in blue displayed AUC>AUG differential cleavage; blue residues with side chains depicted as sticks also showed diminished AUC>AUG cleavage resulting from suppression of cleavage in mRNA(AUC) complexes by the K11C/SE* variant compared to that seen for the K11C variant; while blue residues depicted as spheres also displayed enhanced cleavage in mRNA(AUG) complexes by K11C/SE* and V129C/SE* compared to that given by the K11C and V129C variants, respectively. Gold residues were cleaved constitutively; while cyan residues exhibited enhanced cleavage in AUG versus AUC complexes specifically by the Q73C variant.

start codons (Sui$^-$ phenotype) conferred by SE mutations *in vivo* (10).

Interestingly, the SE* substitutions had a different consequence for cleavage of the adjacent h29 residues G1575 and A1576 by K11C, increasing the extent of cleavage in all three complexes and eliminating the modest AUC>AUG differential cleavage of A1576 displayed by the otherwise WT K11C variant (Figure 3B and Supplementary Figure S6A). (The resulting constitutive pattern of A1576 cleavage observed for K11/SE* is designated by using a gold label for this variant and inserting a gold dot to the left of the A1576 band in the mRNA(AUG) lane of the gels (Figure 3B and Supplementary Figure S6A).) To summarize the result that the SE* substitutions in the K11C/SE* variant diminish AUC>AUG differential cleavage of A1576 by enhancing cleavage in the AUG complex, this residue is depicted with its side chain in 'spheres' representation in addition to blue color in Figure 4. Remarkably, the SE* substitutions also strongly enhanced A1576/G1575 cleavage when introduced into the V129C variant, which confers only low-level cleavage of these residues with WT SE elements present (Figure 3A and B). The fact that the SE* substitutions enhance cleavage of G1575/A1576 directed by Cys residues located in either the NTT (K11C) or CTT (V129C) again seems most consistent with the idea that SE* substitutions evoke a conformational change in the PIC that increases the susceptibility of G1575/A1576 to cleavage. Considering that G1575/A1576 interact with conserved G:C base-pairs in the $tRNA_i$ ASL, we propose that the SE* substitutions eliminate these A-minor interactions and thereby increase exposure of G1575/A1576 to hydroxyl radicals generated from either NTT- or CTT Cys residues in the PIC. This would be consistent with our previous findings that SE* mutations impair AUG recognition and reduce the rate of P_i release from eIF2, in addition to decreasing discrimination against near-cognate start codons (4,10).

It is intriguing that the aforementioned dual effects of SE* substitutions, of decreasing AUG recognition while boosting relative frequencies of near-cognate utilization, are reflected in their opposing effects on cleavage of these adjacent P site residues. We envision that the SE* substitutions suppress cleavage of U1578–A1577 in AUC complexes by enhancing one aspect of the shift to the P_{IN} state of Met-$tRNA_i$ binding at near-cognate start codons to shield these residues from hydroxyl radicals, whereas cleavage of nearby residues G1575/A1576 by the SE* variants is increased in both AUG and AUC complexes owing to reduced A-minor interactions of G1575/A1576 with the $tRNA_i$ ASL. Loss of the A-minor interactions might account for the fact that the SE* substitutions do not appear to increase occupancy of the P_{IN} state for the AUC complexes (Supplementary Figure S4A and B).

P site or A site residues C1634–A1635 and C1637–G1638. The AUC>AUG pattern of cleavage described above was also observed for residues C1634–A1635 and C1637–G1638, located between h44 and h28 and in proximity to the mRNA codons located in the A site (C1634–A1635) or P site (i.e. the AUG codon; residues C1637–G1638) (13,14). Differential cleavage of these residues was observed in comparisons of No-mRNA and mRNA(AUG) complexes for variants K11C, P22C and V69C (Figure 5A), and confirmed in comparisons of mRNA(AUG) versus mRNA(AUC) complexes for all four residues by P22C and V69C, and for C1634/C1637/G1638 for K11C (Figure 5B and Supplementary S7A; quantifications for K11C in Figure 5D). Interestingly, the latter experiments also revealed that the SE* substitutions in the K11C/SE* variant reduced the cleavage of C1634/C1637/G1638 specifically in the mRNA(AUC) complex (Figure 5B and Supplementary Figure S7A, mRNA(AUC), K11C versus K11C/SE*) and thereby diminished the AUC>AUG differential cleavage observed for the K11C variant with WT SE elements. As explained above, SE-dependent AUC>AUG cleavage of C1634/C1637/G1638 is summarized in Figure 4 by depicting their side chains as blue sticks. The fact that AUG recognition diminishes their susceptibility to cleavage in a manner dependent on the SE elements suggests that AUG recognition evokes an altered conformation of the 40S decoding center, or the position of mRNA, that reduces the cleavage susceptibility of 18S rRNA residues contacting the A or P site codons in mRNA.

P site or A site residues U1761 and A1756–G1757. These residues are located in h44 (Figure 6C) and also occur in proximity to the A site codon (A1756–G1757) or P site codon (U1761) in the mRNA (13,14). All three residues display AUC>AUG cleavage for variants K11C, P22C and V69C and the more intense cleavage at AUC is reduced by the SE* substitutions in the K11C/SE* variant (Figure 6A–B and Supplementary Figure S8A; quantification for K11C in Figure 6D; 'blue-sticks' depiction of U1761 and A1756–G1757 in Figure 4). By contrast, the Q73C variant displays AUC>AUG cleavage for A1756 and U1761 but constitutive cleavage of G1757 and U1758 (Figure 6A–B, Q73C, blue and gold dots, respectively, in mRNA(AUG) lanes). Moreover, cleavage of C1759 and G1760 by Q73C is actually enhanced for the AUG versus AUC and No-mRNA complexes (Figure 6A–B, Q73C, cyan dots in mRNA(AUG) lanes). Hence, in the PIC structures of Figure 4, residue U1758 is colored gold to designate constitutive cleavage whereas C1759–G1760 are shown in cyan to designate their AUG-enhanced cleavage by the Q73C variant.

It is noteworthy that residues A1755 and A1756 are juxtaposed with loop residues in the β1–β2 hairpin of the OB-fold of eIF1A (12,13), and that A1756 rearranges from a 'stacked-in' to a 'flipped out' base conformation in the presence of eIF1 (11), which implies that eIF1 dissociation from the 40S subunit on AUG recognition would favor the stacked-in conformation of A1756. This last inference would help to explain the reduced cleavage of A1756 seen in the AUG versus AUC/No-mRNA complexes, as eIF1 has been shown to dissociate more rapidly from complexes with AUG versus non-AUG start codons (3), and the resulting stacked-in conformation of A1756 could render it less susceptible to cleavage. The enhanced cleavage of C1759–G1760 by the Q73C variant specifically in the AUG complex (Figure 6) could also be explained by eIF1 dissociation, as these residues are predicted to contact eIF1 (11–14). This proposal is further supported by the fact that the Q73C variant also frequently produced AUG-enhanced cleavage of another set of residues on the opposite strand

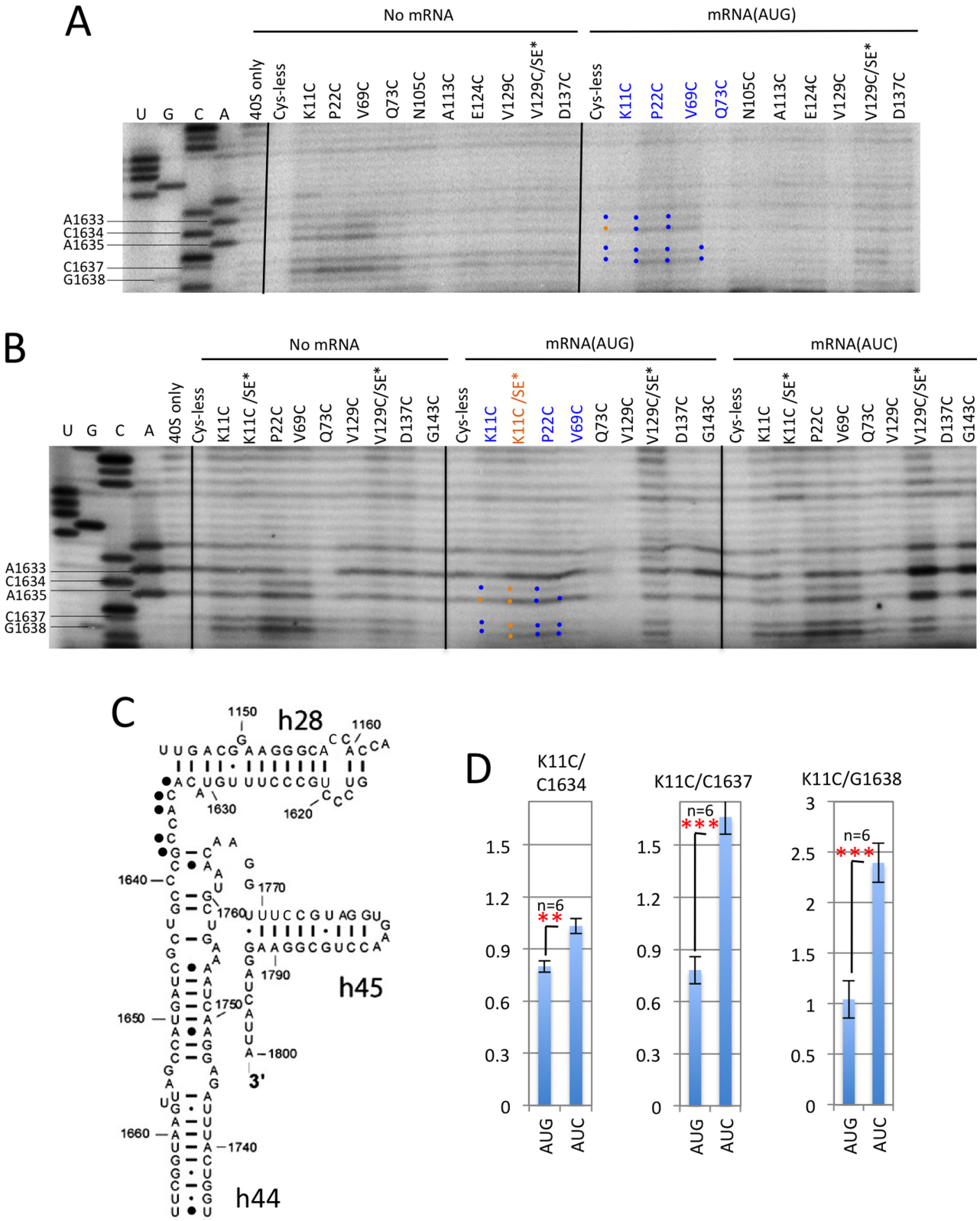

Figure 5. DHRC of P-site and A-site residues between h44 and 28 by eIF1A variants K11C, P22C, V69C and Q73C is modulated by start codon recognition. (**A–C**) Sites of cleavage of 18S rRNA by eIF1A single-Cys variants in PICs assembled with no mRNA, mRNA(AUG) or mRNA(AUC) mapped by primer extension inhibition, as described in Figure 3. (**D**) Cleavage of the indicated residues by the K11C derivative was quantified as described in Figure 3D.

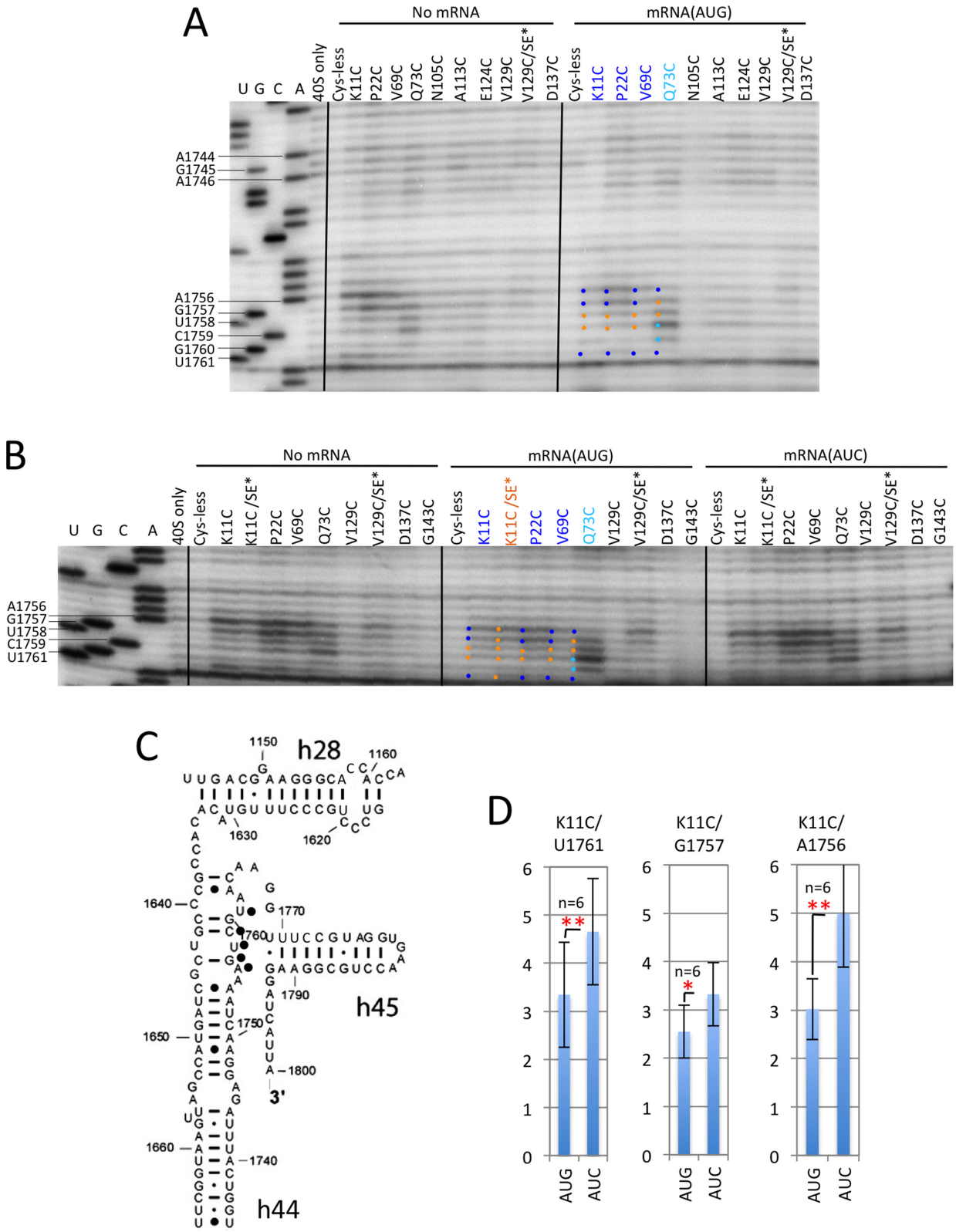

Figure 6. DHRC of P-site and A-site residues in h44 by eIF1A variants K11C, P22C, V69C, and Q73C is modulated by start codon recognition. (**A**–**C**) Sites of cleavage of 18S rRNA by eIF1A single-Cys variants in PICs assembled with no mRNA, mRNA(AUG) or mRNA(AUC) mapped by primer extension inhibition, as described in Figure 3. Cyan dots to the left of bands indicate enhanced cleavages in the AUG versus AUC or No-mRNA complexes. (**D**) Cleavage of the indicated residues by the K11C derivative was quantified as described in Figure 3D, except that data from two experiments comparing mRNA(AUG) to No-mRNA complexes were included with the mRNA(AUG) versus mRNA(AUC) comparisons.

of h44, U1643–C1646 (Supplementary Figure S8B and C; cyan dots), which are likewise in proximity to eIF1 (11,14). Although this interpretation does not readily explain why cleavage of C1759–G1760 is enhanced only for Q73C and not for the K11C, P22C and V69C variants, we note that the latter variants cleave C1759 at levels only slightly above background and do not cleave G1760 at all. Thus, on balance, it seems likely that cleavages in h44 directed by Q73C are enhanced, at least in part, by greater eIF1 dissociation from the AUG versus AUC complex.

Evidence for SE-dependent ejection of the CTT from the P-site on AUG recognition

As noted above, we observed cleavage of P-site residues C1461, G1462 and C1463 in h30 for all of the eIF1A variants (Figure 2A–D and Supplementary Figure S5A–C), and these residues are close to the ASL of $tRNA_i$ (13,14) (Figure 2A, cyan spheres). Unlike the other cleavages in the decoding center discussed above, the intensities of C1461/G1462/C1463 cleavage were not suppressed in the AUG PICs for the NTT derivatives K11C and P22C and OB-fold derivative V69C, displaying essentially constitutive cleavage in the three different PICs (Figure 7A and C; gold dots). These findings suggest that rearrangement from the P_{OUT} to P_{IN} states does not significantly reduce the accessibility of these three P site residues to hydroxyl radicals generated from sites in the NTT or OB-fold. It is intriguing, however, that cleavage of C1463 was clearly suppressed in the AUG PIC for all four CTT variants E124C, V129C, D137C and G143C, and by a fifth CTT variant (A113C) not mentioned above (Figure 7B and C, blue dots). Cleavage of G1462 was also suppressed in the AUG complex for CTT variants D137C and G143C (Figure 7B). Moreover, the suppression of C1463 cleavage in the AUG complex by the V129C variant was eliminated by the SE* mutations (Figure 7B, blue dot to gold dot transition for V129C versus V129C/SE* lanes for C1463). Thus, residues G1462 and C1463 are depicted as 'blue-only' and 'blue-spheres', respectively, in Figure 4.

Having just concluded on the basis of constitutive cleavage of these h30 residues by NTT and OB-fold Cys variants that they are equally accessible to hydroxyl radicals in the AUG and AUC PICs, the AUG-specific suppression of C1463 and G1462 cleavage by CTT Cys residues seems most consistent with the idea that the position of the CTT is adjusted in the AUG complex in a manner that moves the CTT Cys residues further away from P site residues in h30. This is in accordance with predictions that the mammalian CTT would clash with the $tRNA_i$ ASL when the latter binds deeply in the P site (15), and the demonstration that the CTT moves away from eIF1 and closer to the N-terminal domain (residues 1-170) (NTD) of eIF5 on AUG recognition to enable P_i release (4). Thus, we propose that AUG recognition evokes ejection of the CTT from its location deep in the P site and its subsequent movement toward the 40S head domain, which specifically reduces cleavage of C1463 by the CTT Cys residues because it is located deeper in the P site than are G1462 and C1461 (Supplementary Figure S9A). From the postulated adjusted location of the CTT, C1461 would be cleaved most efficiently in the AUG complex because it is the only one of the three residues that is highly exposed from the vantage point of the 40S head domain (Supplementary Figure S9B). The constitutive cleavage of all three residues in the AUG complex conferred by Cys residues in the OB-fold or NTT could be explained by noting that all three residues are equally exposed from the vantage point of the OB-fold of eIF1A (Supplementary Figure S9A).

The Q73C variant was unique in conferring AUG enhanced cleavage of all three of these h30 residues (Figure 7A and C). This might reflect the fact that rotation of the 40S head in the AUG complex brings these h30 residues (in the 40S head) closer to Q73C (near the 40S body) (13,14).

Evidence for a conformational change in the mRNA entry channel on AUG recognition

In addition to specific residues near the decoding sites discussed above, certain residues in proximity to the mRNA entry channel and entry channel latch also exhibit SE-dependent AUC>AUG cleavage. Thus, K11C, P22C and V69C all conferred specific cleavage of h34 residues A1425–C1426 and G1428–G1429 to a greater extent in the No-mRNA and AUC PICs versus the AUG PICs, with the strongest cleavage occurring at G1428 (Figure 8A–C, K11C quantification in Supplementary Figure S10C). Moreover, the SE* substitutions diminished cleavage of all four residues in the mRNA(AUC) complex by the K11C/SE* variant compared to K11C (Figure 8A–C). These residues are located in the portion of the 40S head that forms the mRNA entry channel (Figure 4, blue sticks). The AUC>AUG pattern of cleavage was also observed with the P22 and V69C variants for h34 residues C1439–G1440 (Figure 8A and Supplementary Figure S10A and B), which belong to the portion of the entry channel latch located in the 40S head domain; however, cleavage by K11C was too weak to determine whether the SE* substitutions suppress cleavage of these residues in the AUC complex in the manner described for other cleavages exhibiting AUC>AUG cleavage. (Hence, residues C1439–G1440 are depicted as 'blue-only' without showing side chains in Figure 4.) Cleavage of the adjacent latch residues C1441–U1442 was constitutive (Figure 8A and Supplementary Figure S10A and B). The h34 residues 1271–1276 also form part of the entry channel latch, and residues G1271, G1273, C1274 and U1276 in this stretch of nucleotides exhibit constitutive cleavage by the V69C variant (Supplementary Figure S10E; Figure 4, gold depiction). Although it was unresolved whether these last residues display AUC>AUG cleavage by K11C, their cleavage was consistently suppressed by the SE* substitutions in the K11C/SE* variant for both AUG and AUC complexes (Supplementary Figure 10E).

Residues in h18 comprise the portion of the entry channel latch located in the 40S body, and also line the bottom of the mRNA entry channel. Residues G574–C575 in the entry channel exhibit AUC>AUG cleavage for K11C, P22C and V69C, with the SE* substitutions specifically reducing cleavage at AUC by the K11C/SE* variant (Figure 9A–C and Supplementary Figure S11A-C; blue sticks in Figure 4). By contrast, we observed strong constitutive cleavage of residues U578–A580, which form the latch-proper

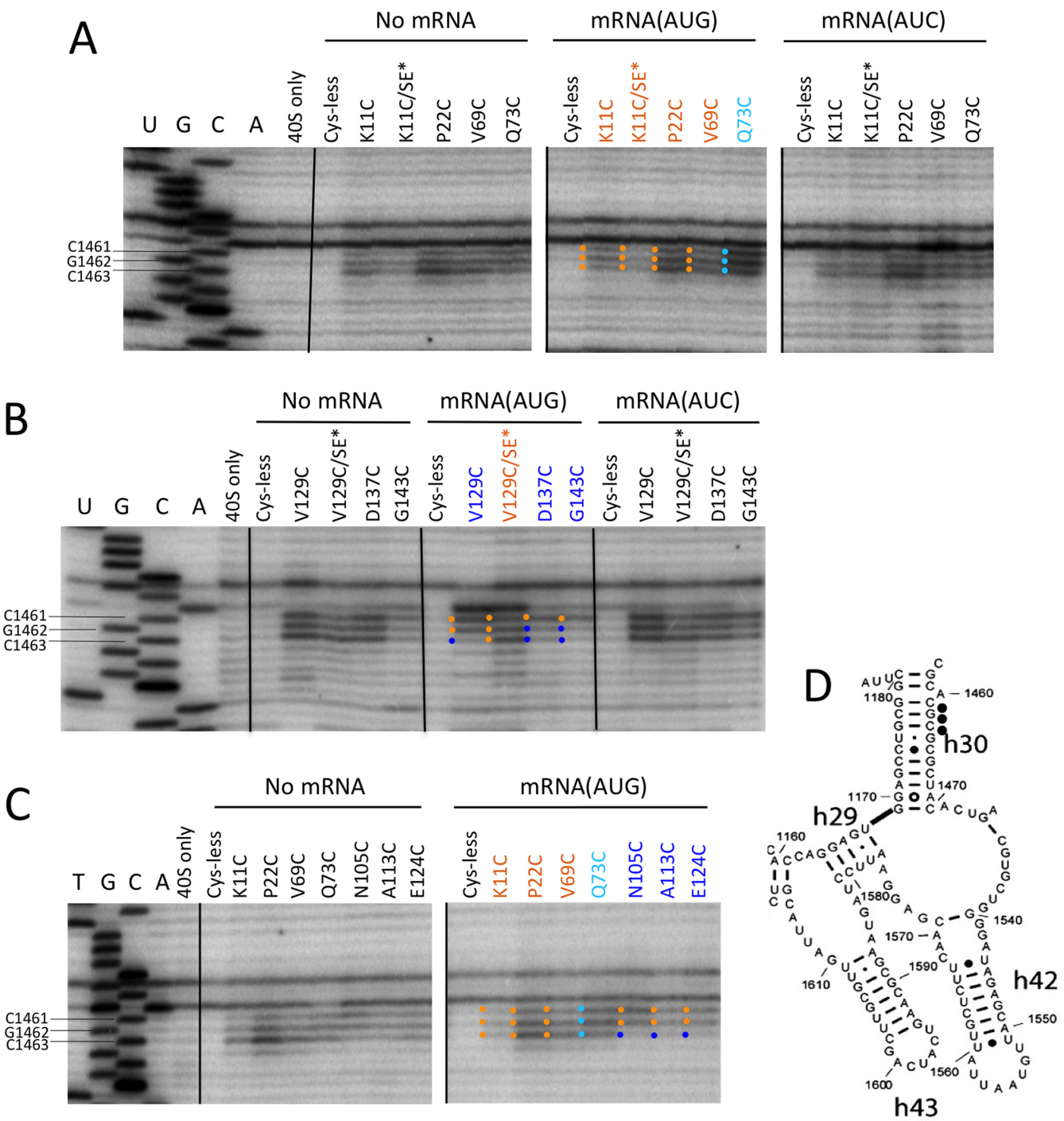

Figure 7. DHRC of P-site residues in h30 by eIF1A variants with CTT-located cysteines is modulated by start codon recognition. (**A–D**) Sites of cleavage of 18S rRNA by eIF1A single-Cys variants in PICs assembled with no mRNA, mRNA(AUG) or mRNA(AUC) mapped by primer extension inhibition, as described in Figures 3 and 6.

in the 40S body, for variants P22C and V69C, and lesser constitutive cleavage for K11C (Figure 9A–C and Supplementary Figure S11A; Figure 4, gold depiction). While the SE* substitutions appear to reduce cleavage of U578–A580 by K11C in the K11C/SE* variant, this did not apply selectively to the AUC complexes, which is similar to the non-canonical behavior noted above for h34 latch residues G1271, G1273, C1274 and U1276. A third pattern of cleavage was observed for residues G552–G553 and U558–C559, located near the entry channel, which entailed AUC>AUG cleavage by K11C, P22C and V69C, with no clear effect of the SE* substitutions on cleavage directed by K11C in either the AUC or AUG complexes (Figure 9A–C and Supplementary Figure S11A-C and B; Figure 4, blue-only depiction).

Despite the complexities in the cleavage patterns for residues in h34 and h18 described above, our findings of

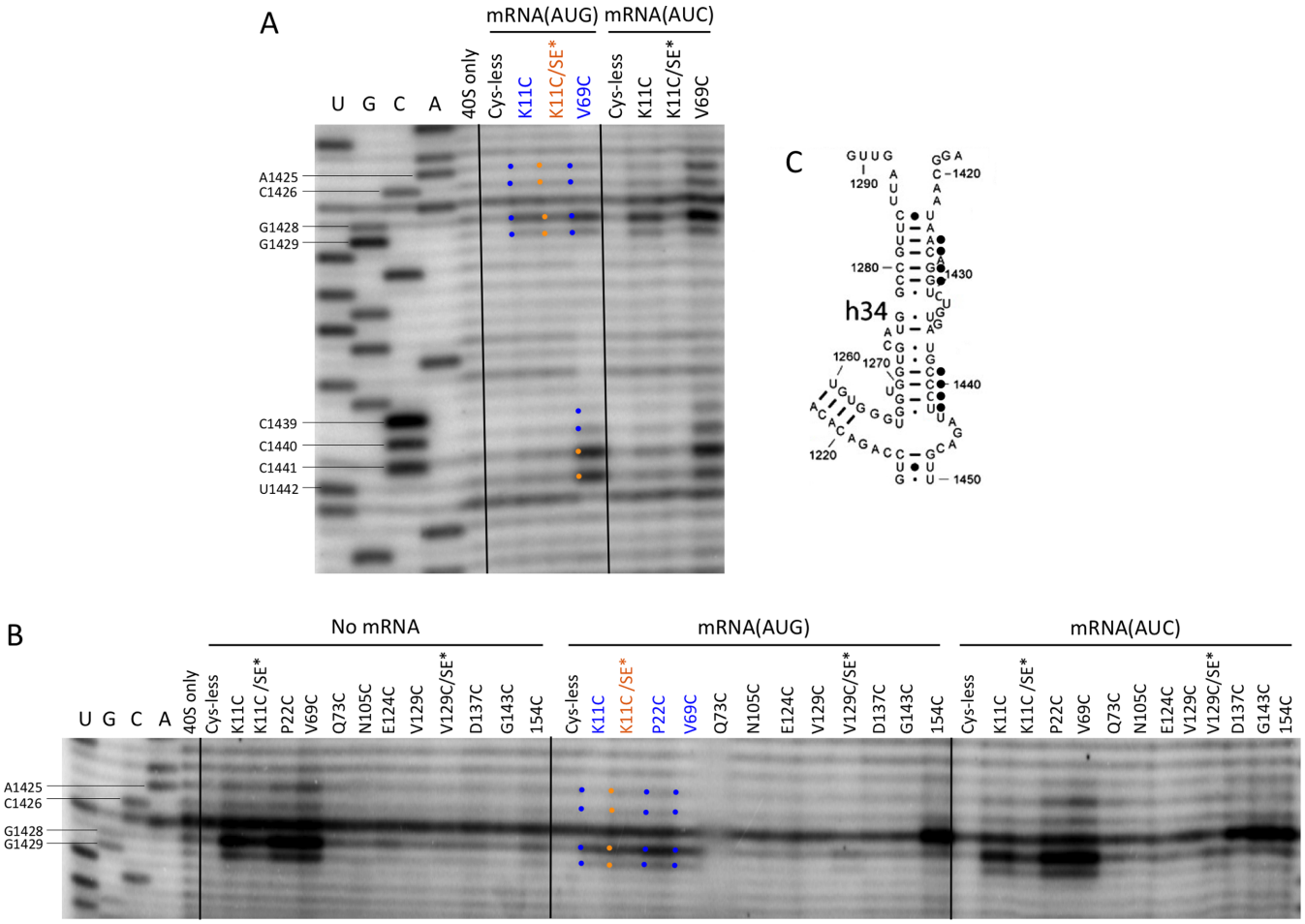

Figure 8. DHRC of h34 residues in the upper-entry channel or latch region by eIF1A variants K11C, P22C and V69C is modulated by start codon recognition. (**A–C**) Sites of cleavage of 18S rRNA by eIF1A single-Cys variants in PICs assembled with no mRNA, mRNA(AUG) or mRNA(AUC) mapped by primer extension inhibition, as described in Figure 3.

AUC>AUG cleavage for several residues in the top (h34) or bottom (h18) portions of the mRNA entry channel, or in the h34 or h18 portions of the entry channel latch, suggest that AUG recognition evokes a conformational change in the entry channel and latch, or alters the position of mRNA in the entry channel, in a manner that reduces the accessibility of these residues to hydroxyl radicals. We speculate that the constitutive cleavage of the lower latch residues in h18 (U578–A579) reflects their strong exposure to hydroxyl radicals produced by the NTT cysteines and V69C, as they are highly solvent-exposed and display the most intense cleavages conferred by any of the Cys residues examined here. This high-level cleavage might obscure subtle differences in the exposure of these residues associated with conformational changes evoked by AUG recognition or SE* substitutions in the eIF1A CTT.

DISCUSSION

In this study, we set out to test the hypothesis that AUG recognition evokes displacement of the CTT from the P site to accommodate the P_{IN} state of Met-$tRNA_i$ binding. We observed that each of five different eIF1A derivatives with single Cys residues in the CTT conferred specific cleavages of only three h30 residues, C1461/G1462/C1463, located in the P site in proximity to the lower portion of the ASL helix of $tRNA_i$. Cleavage of C1463, which is deepest in the P site, was specifically suppressed in the AUG complexes for all five CTT single-Cys variants; whereas cleavage of C1461, which occupies a more exposed position (Figure 4 and Supplementary Figure S9A and B), was cleaved constitutively by these same eIF1A variants. By contrast, all three h30 residues were cleaved constitutively by different eIF1A derivatives containing Cys residues in the NTT or OB-fold. These findings are in accordance with previous proposals that the CTT reaches deep into the P site in the open/P_{OUT} complex formed with mRNA(AUC) but is prevented from doing so in the closed/P_{IN} state formed with mRNA(AUG) owing to a clash with the $tRNA_i$ ASL, and hence moves to a new location in the PIC (Figure 10A and B, arrow 4) (10,15). The movement of the CTT away from the P site on AUG recognition would then reduce cleavage of C1463, but the more exposed residue C1461 would remain highly susceptible to hydroxyl radicals generated by CTT Cys residues. Consistent with this interpretation, an intermediate set of results was obtained for the middle residue, G1462, which displayed constitutive cleavage for three CTT variants but

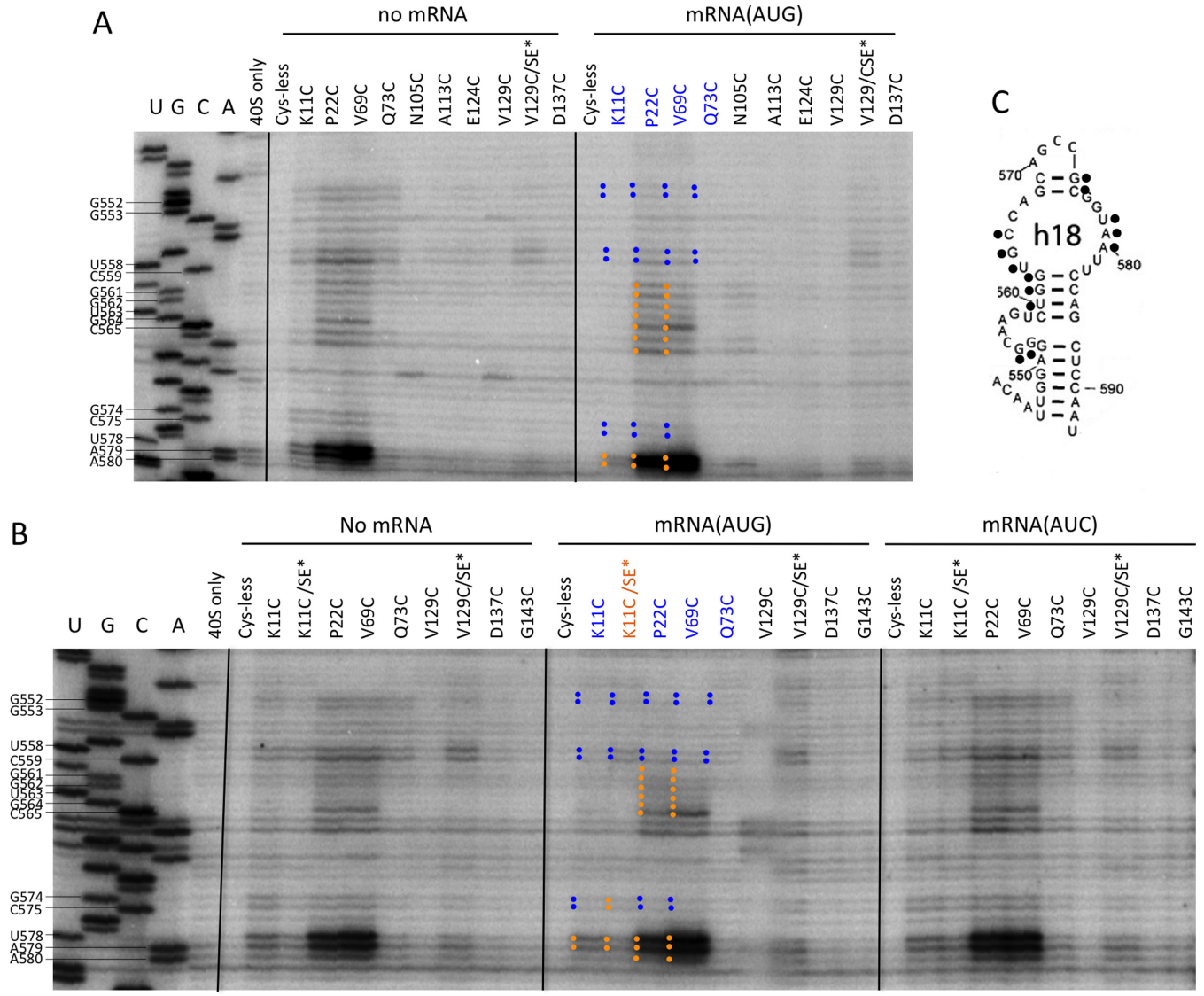

Figure 9. DHRC of h18 residues in the lower entry channel or latch region by eIF1A variants K11C, P22C, V69C and Q73C is modulated by start codon recognition. (**A–C**) Sites of cleavage of 18S rRNA by eIF1A single-Cys variants in PICs assembled with no mRNA, mRNA(AUG) or mRNA(AUC) mapped by primer extension inhibition, as described in Figure 3.

AUC>AUG cleavage for the remaining two CTT variants. By contrast, the constitutive cleavage of all three residues directed by OB-fold or NTT derivatives would be explained by noting that C1461/G1462/C1463 are equally exposed from the vantage point of the OB-fold (Supplementary Figure S9A). Given that the eIF1A CTT moves toward the eIF5-NTD on start codon recognition (4), an attractive possibility is that movement of the CTT from the P site in the mRNA(AUG) complex enables its interaction with the eIF5-NTD positioned in the 40S head (Figure 10B), and from this new location, hydroxyl radicals generated by CTT Cys residues more readily attack the h30 residue (C1461) that is most exposed from this vantage point in the PIC.

It is intriguing that the presence of the SE* substitutions in the V129C/SE* variant eliminated the suppression of C1463 cleavage in the AUG complex seen for V129C. The fact that V129C/SE* behaves identically to the aforementioned derivatives with NTT or OB-fold Cys residues in conferring constitutive cleavage of all three h30 residues can be explained by proposing that the SE* substitutions evoke an aberrant location of the CTT, moving it from the P site to a location closer to the OB-fold. In fact, we concluded previously that the SE* substitutions displace the CTT from the P site in order to account for their dual effects of (i) impairing the CTT interaction with the eIF5 NTD that is required to trigger dissociation of P_i from eIF2-GDP·P_i at AUG codons and (ii) enabling the transition to P_{IN} at near cognates (Sui^- phenotype) by mitigating the predicted clash between the CTT and Met-$tRNA_i$ in the P-site (4). The fact that the CTT Cys residues do not direct cleavage of P-site residues G1575–U1578, which were cleaved by other single-Cys variants, might be explained by noting that these rRNA residues (located in h29) contact a different face of the $tRNA_i$ ASL helix than that contacted by h30 residues

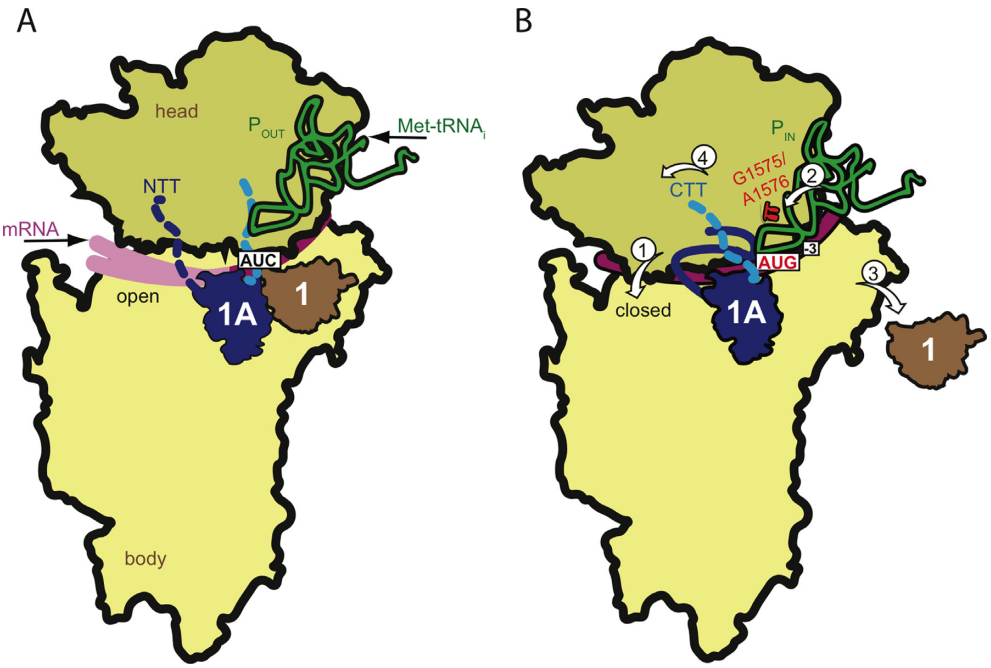

Figure 10. Schematic summary of conformational differences between PICs assembled with mRNA (AUC) versus mRNA(AUG) deduced by differential hydroxylradical cleavage of 18S rRNA residues directed by Fe(II)-BABE derivatives of single-Cys variants of eIF1A. (**A–B**) Contours of components of the py48S complex (14) were drawn and modified by removing (for simplicity) the eIF2 subunits, depicting hypothetical unresolved locations of the unstructured eIF1A NTT and CTT as dotted blue or cyan lines, and removing eIF1 from the PIC to depict its dissociation on AUG recognition (in panel B). In (A), the relative orientation of the 40S head and body were manually altered to depict a wider mRNA entry channel and more open-latch configuration; and the segment of mRNA occupying the entry channel was shown with a lighter hue and in two different locations to depict its greater mobility in the mRNA binding cleft with an AUC in the P site. Conformational rearrangements in the transition between the P_{OUT} (A) and P_{IN} (B) complexes revealed in this study are depicted by the four white arrows in (B). (1) A more constricted mRNA entry channel and closed latch configuration, and/or tighter binding of mRNA in the entry channel, in the AUG complex (B) versus AUC complex (A) is indicated by the reduced cleavage of entry channel and latch residues, and of A-site and P-site residues in proximity to the mRNA, observed in the AUG versus AUC complexes by eIF1A variants harboring single-Cys residues in either the NTT or OB-fold. (2) Similar results for P site residues, including G1575/A1576 that interact directly with the ASL (red symbols in (B)), provide evidence for movement of Met-tRNA$_i$ from the P_{OUT} conformation (A) deeper into the P site for the P_{IN} state (B) on AUG recognition. (3) By contrast, enhanced cleavage of residues at the eIF1 binding site in the AUG versus AUC complexes directed by the Q73C variant is consistent with dissociation of eIF1 from the platform on AUG recognition. (4) Movement of the CTT on AUG recognition from its location near the P site (A) is inferred from the reduced cleavage of P site residues G1462/G1463 in the AUG versus AUC complexes observed only for eIF1A variants with Cys residues in the CTT. Based on the suppression of cleavages in the mRNA binding cleft and latch specifically for AUC complexes provoked by the SE* substitutions in the eIF1A CTT, these substitutions appear to favor rearrangement to the closed conformation of the entry channel and latch depicted in (B) even at the near-cognate AUC codon, consistent with their Sui$^-$ phenotype *in vivo* (10). By contrast, the effect of the SE* substitutions of enhancing cleavage of G1575/A1576 in the AUG complex suggests that these substitutions disfavor the direct interactions of G1575/A1576 with the tRNA$_i$ ASL depicted in (B), even at AUG codons, consistent with their ability to disrupt interaction of the CTT with the eIF5 GAP domain and P_i release on AUG recognition (4). Schematics were modified from those in Figure 7 of Hussain et al (14).

G1462–C1463 (Figure 4), such that the path to h29 of free radicals generated from CTT Cys residues from the proposed location of the CTT near h30 would be obstructed by the tRNA$_i$ ASL. Finally, the finding that the SE* version of the CTT variant V129C behaves exceptionally by conferring cleavage of h29 residues G1575–A1576 could be explained by our proposal that SE* substitutions eliminate A-minor interactions of these h29 residues with the tRNA$_i$ ASL and that the altered location of the CTT conferred by the SE* substitutions provides a clear path to this portion of the P site by hydroxyl radicals generated by V129C/SE*.

The h30 cleavage sites just discussed were unique in displaying suppression of cleavage in AUG versus AUC PICs only for the subset of eIF1A variants with Cys residues in the CTT. By contrast, the NTT derivatives K11C and P22 and OB-fold derivative V69C conferred AUC>AUG differential cleavage of numerous other rRNA residues located in the decoding sites and entry channel. As it seems unlikely that Cys residues in both the NTT and OB-fold would alter their locations in the PIC between AUC and AUG complexes in the manner proposed above for the CTT Cys residues, we instead attribute their AUC>AUG cleavage patterns to a conformational rearrangement of the PIC evoked by start codon recognition that reduces access of hydroxyl radicals to the affected rRNA residues. Supporting this interpretation, the presence of the SE* substitutions in the NTT variant K11C generally suppressed cleavage in the AUC complex and rendered it more similar in intensity to the AUG complex, consistent with the ability of the SE* substitutions to enhance transition to the closed conformation at near-cognate start codons *in vivo* (Sui$^-$ phenotype). This stereotypical pattern of AUC>AUG cleavage mitigated by SE* substitutions in K11C was observed for all of the residues in the decoding center or mRNA entry channel depicted in blue stick format in Figure 4.

Our finding that this pattern of SE-dependent AUC>AUG cleavage was observed for four adjacent residues in h29 that directly contact the ASL helix, G1575/A1576/A1577/U1578, supports the idea that Met-tRNA$_i$ binds deeper in the P site, with G1575–A1576 interacting with G:C base pairs in the ASL, to stabilize Met-tRNA$_i$ binding and achieve the P$_{IN}$ state at the AUG codon (Figure 10A and B, arrow 2). Indeed, a comparison of the recent cryo-EM structures of the yeast 40S·eIF1·eIF1A and yp48S complexes predicts a substantial movement of residues G1575–A1576 toward the tRNA$_i$ ASL in the transition from an open, scanning conformation to the closed/P$_{IN}$ state, enabling interaction of G1575–A1576 with the ASL G:C base pairs (14). Interestingly, the SE* substitutions increased G1575–A1576 cleavage, particularly in the AUG complex, conferring a constitutive pattern of cleavage, which might result from G1575–A1576 becoming at least partially disengaged from the ASL G:C pairs and, hence, more susceptible to cleavage. Thus, while the SE* substitutions appear to allow deeper binding of Met-tRNA$_i$ in the P site at near-cognate codons, reducing cleavage of A1577–U1578 in AUC complexes, they also appear to disengage G1575–A1576 from the ASL G:C base pairs at both AUG and AUC start codons. This dual effect on the conformation of h29 residues helps to explain how the SE* substitutions impair P$_i$ release from eIF2 at AUG codons in reconstituted PICs (4) while also elevating UUG initiation *in vivo* (10). Thus, our cleavage data support the postulates that tRNA$_i$ is more fully engaged with the P site in the P$_{IN}$ versus P$_{OUT}$ states and that A-minor interactions of G1575–A1576 with conserved ASL G:C base pairs participate in stabilizing P$_{IN}$ on AUG recognition.

SE-dependent AUC>AUG cleavage was also observed for residues between h28 and h44 located in proximity to the AUG codon in the P site (C1637–G1638) or the adjacent A site codon of the mRNA (C1634-A1635). Because these residues are close to the mRNA, it is possible that the more stable codon:anticodon duplex formed with AUG causes the A site codon, as well as the AUG itself in the P site, to become more 'locked-in' to the mRNA binding cleft in a way that blocks access of hydroxyl radicals to these 18S rRNA residues. The same interpretation could apply to the SE-dependent AUC>AUG cleavage observed for residues in h44 predicted to be near the A site (A1756-G1757) or P site codon (U1761), except that the reduced cleavage of A1756 in the AUG complex could also arise from dissociation of eIF1 on AUG recognition. As noted earlier, A1756 assumes a 'flipped out' base conformation on eIF1 binding (11), which could render it more susceptible to cleavage in the AUC complex in which eIF1 is more tightly bound, but less susceptible to cleavage in the AUG complex with eIF1 weakly bound. Selective dissociation of eIF1 from the AUG complex would also explain several instances of enhanced cleavage in AUG complexes conferred by the Q73C variant, as the relevant residues (C1759–G1760 and G1643-C1646) are located proximal to the eIF1 binding site. Thus, our cleavage data also support the postulate that AUG recognition evokes dissociation of eIF1 from its binding site on the 40S platform (Figure 10A and B, arrow 3).

In addition to residues located proximal to the A or P sites, residues in the mRNA entry channel displayed stereotypical SE-dependent AUC>AUG hydroxyl radical cleavage. These include constituents of both h34 (A1425–C1426 and G1428–G1429) and h18 (G574–C575) located in the upper or lower portions, respectively, of the mRNA entry channel (Figure 4). Additional h18 residues located near the entry channel latch (G552–G553 and U558–C559), and h34 residues belonging to the latch-proper (C1439–C1440), also displayed AUC>AUG cleavage, although evidence for SE-dependence was lacking for these residues (Figure 4). One way to interpret these findings is to propose that the presence of a non-AUG codon in the P site is associated with an open, or only partially closed, latch conformation that is conducive to scanning with TC in the P$_{OUT}$ state. As suggested previously (13), partial latch closure could be required in the open/P$_{OUT}$ state to ensure the processivity of scanning. AUG recognition would then elicit a more closed conformation of the latch that, together with a perfect codon:anticodon duplex in the P site, arrests scanning and allows sufficient time for P$_i$ release from eIF2 and dissociation of eIF2-GDP from Met-tRNA$_i$. In this view, the AUC>AUG cleavage of other h34 and h18 residues located in the upper and lower portions of the mRNA entry channel itself, A1425–G1429 and G574–C575 (Figure 4), could result from a narrower mRNA binding cleft in the closed/P$_{IN}$ versus open/P$_{OUT}$ conformations that restricts access of hydroxyl radicals to these 18S rRNA residues (Figure 10A and B, arrow 1). As noted above, rather than a conformational change in the entry channel and latch, it could be proposed instead that the mRNA becomes more tightly fixed in the mRNA binding cleft as the result of the more stable codon:anticodon base pair afforded by AUG in the P$_{IN}$ state, thereby shielding rRNA residues in proximity to the mRNA from hydroxyl radicals. The mRNA in the AUC complex, by contrast, would be more mobile and provide less protection from cleavage. The proposed weaker association of the mRNA with the entry channel would be conducive to scanning. Examination of the yp48S PIC structure (14) reveals that 8 of the 10 entry channel residues listed above that exhibit AUC>AUG cleavage are between 7 Å and 14 Å away from the mRNA, and the latch residues are even more distant from the mRNA. Thus, fixing the mRNA in the entry channel might not be able to protect residues located in both the upper (h34) and lower (h18) portions of the entry channel simultaneously without some constriction of the channel or closure of the latch on AUG recognition. Such conformational changes could be provoked by rotation of the 40S head relative to the body (13,14).

An alternative explanation for the increased cleavage of entry channel residues in the AUC complex would be that the PIC dissociates completely from the mRNA more frequently in the AUC versus AUG PIC to provide an unobstructed path of hydroxyl radicals to the entry channel. In fact, the rate constant for TC dissociation from the PIC is ~3-fold higher for AUC versus AUG complexes, and dissociation of the TC from the PIC might also evoke mRNA dissociation from the 40S subunit. However, several considerations argue against this explanation for the AUC>AUG pattern of cleavage. First, the rate of TC dissociation from reconstituted PICs is very low, even for AUC complexes (0.67 h^{-1}) (28), compared to the time of exposure to hydroxyl radicals in our experiments (10 min). In addition,

we have repeated all of the cleavage reactions using a 10-fold higher concentration of AUC mRNA. The results of these control experiments, presented in Supplementary Figures S12–S15, revealed no suppression of any AUC>AUG cleavages in PICs assembled at a 10-fold higher concentration of mRNA(AUC). If dissociation of mRNA was responsible for the greater cleavage in AUC complexes, then increasing the mRNA(AUC) concentration should increase the rate of mRNA binding to the PIC and decrease the lifetime of the hypothetical complexes lacking mRNA to suppress cleavages in the AUC complex. Second, greater dissociation of mRNA(AUC) would not explain the reduced cleavage in AUG complexes of residues G1428–G1429 in the upper-entry channel and of latch residues C1439–C1440 because the mRNA does not lie between these residues and eIF1A in the yp48S structure (14) (Figure 4) and, hence, mRNA should not obstruct the path of hydroxylradicals to these residues. Third, the SE* substitutions in the K11C variant destabilize the PIC at AUG (Supplementary Figure S4A, cf. K11C and K11C/SE* for mRNA(AUG)), and would be expected to increase the frequency of mRNA dissociation from the AUG complexes; however, the K11C and K11C/SE* derivatives confer similar low-level cleavage of upper-entry channel residues A1425–G1429 (Figure 8B) and lower-entry channel residues G574–C575 (Figure 9B) in the AUG complexes. Hence, while we cannot completely rule out the possibility that a higher off-rate of mRNA from the AUC versus AUG complex is responsible for the AUC>AUG pattern of cleavage, we consider it more likely that AUG recognition evokes a more constricted conformation of the entry channel and latch, fixes the mRNA in the entry channel or evokes both effects, in a way that restricts access of hydroxyl radicals to rRNA residues in these structural elements of the 18S rRNA.

To evaluate further this last conclusion, we compared the conformations of the entry channel and latch residues in the yp48S PIC and yeast 40S-eIF1-eIF1A complexes of Hussein *et al.* (14), assuming that they represent, respectively, the closed/P_{IN} state formed with mRNA(AUG) and an approximation of the open/P_{OUT} state for the mRNA(AUC) complex. These two complexes differ by a 5° rotation of the 40S head relative to the body, which adjusts the position of h34 relative to h18. As a consequence, h34 residues located in the upper portion of the entry channel, including residues A1425–C1426, G1428–G1429 and C1274-U1276 move 3–4 Å closer to residues +6 to +10 of the mRNA (relative to the ATG at +1). As the separation between these mRNA residues and h18 residues in the lower portion of the entry channel is essentially unchanged in the two complexes, the entry channel of the yp48S PIC is narrowed somewhat compared to that seen in the 40S-eIF1-eIF1A complex. In addition, the entry channel latch exhibits more extensive interactions in the yp48S PIC versus the 40S-eIF1-eIF1A complex, as follows. In addition to contacts involving residues in h34 (C1439–C1440) and Rps3 (R143, A144, A145) in the head domain with h18 residues in the body (U578–A579), additional interactions between head and body are seen in the yp48S PIC, including two sets of h34:h18 interactions (U1272/A1275:A579 and C1441/C1440:G562/G561) and an h18:Rps3 interaction (U558:R143/A144). These more extensive interactions between head and body in the yp48S PIC might help to explain the greater protection of latch residues from hydroxyl radical cleavage (C1439–C1440) in the AUG versus AUC complexes. One cautionary note is that superimposition of the cryo-EM structure of the mammalian 43S·DHX29 PIC (lacking mRNA and presumably representing the open/P_{OUT} state) (32) with the yp48S complex (14) reveals a similar rotation of the 40S head, and thus most likely similar entry channel dimensions and latch configurations, in the two structures (T. Hussein and V. Ramakrishnan, personal communication). However, it cannot be excluded that the presence of DHX29 evokes head rotation in the absence of codon-anticodon pairing at AUG in the 43S·DHX29 complex. More generally speaking, it is possible that the conformational changes in the entry channel and latch deduced from our experiments with reconstituted PICs in solution have not been fully captured by any available PIC structures.

As summarized in Figure 10, the results of our experiments provide strong support for the idea that AUG recognition by the TC evokes a more extensive interaction of Met-$tRNA_i$ with the P site (P_{OUT} to P_{IN} transition), displacement of the eIF1A CTT from the P site to accommodate the P_{IN} state, and dissociation of eIF1 from the 40S platform—all key aspects of the current model for the structural rearrangements that occur when the scanning PIC encounters an AUG codon. They also provide new evidence suggesting that this transition also involves a conformational change in the mRNA entry channel and entry channel latch that restricts mRNA movement and thereby promotes the arrest of scanning at the start codon.

SUPPLEMENTARY DATA

Supplementary Data are available at NAR Online.

ACKNOWLEDGEMENTS

We thank Tom Dever, Jon Lorsch and members of our laboratories for many helpful suggestions during the course of this work, and Tom Dever for comments on the manuscript. We also thank Tanweer Hussain, Jose Llácer and Venki Ramakrishnan for communicating results prior to publication, and for helping in preparing Figure 10.

FUNDING

Intramural Research Program of the NIH [GM62128 to Jon R. Lorsch and J.N.]; Department of Science and Technology, Government of India [Int/NZ/P-2/13 to A.K.S.]. Funding for open access charge: Intramural Research Program of the National Institutes of Health.
Conflict of interest statement. None declared.

REFERENCES

1. Hinnebusch,A.G. (2011) Molecular mechanism of scanning and start codon selection in eukaryotes. *Microbiol. Mol. Biol. Rev.*, **75**, 434–467.
2. Hinnebusch,A.G. (2014) The scanning mechanism of eukaryotic translation initiation. *Annu. Rev. Biochem.*, **83**, 779–812.
3. Maag,D., Fekete,C.A., Gryczynski,Z. and Lorsch,J.R. (2005) A conformational change in the eukaryotic translation preinitiation complex and release of eIF1 signal recognition of the start codon. *Mol. Cell*, **17**, 265–275.

4. Nanda,J.S., Saini,A.K., Munoz,A.M., Hinnebusch,A.G. and Lorsch,J.R. (2013) Coordinated movements of eukaryotic translation initiation factors eIF1, eIF1A, and eIF5 trigger phosphate release from eIF2 in response to start codon recognition by the ribosomal preinitiation complex. *J. Biol. Chem.*, **288**, 5316–5329.
5. Algire,M.A., Maag,D. and Lorsch,J.R. (2005) Pi release from eIF2, not GTP hydrolysis, is the step controlled by start-site selection during eukaryotic translation initiation. *Mol. Cell*, **20**, 251–262.
6. Passmore,L.A., Schmeing,T.M., Maag,D., Applefield,D.J., Acker,M.G., Algire,M.A., Lorsch,J.R. and Ramakrishnan,V. (2007) The eukaryotic translation initiation factors eIF1 and eIF1A induce an open conformation of the 40S ribosome. *Mol. Cell*, **26**, 41–50.
7. Pestova,T.V., Lorsch,J.R. and Hellen,C.U.T. (2007) The Mechanism of Translation Initiation in Eukaryotes. In: Mathews,M., Sonenberg,N. and Hershey,J.W.B. (eds), *Translational Control in Biology and Medicine*. Cold Spring Harbor Laboratory Press, Cold Spring Harbor, pp. 87–128.
8. Fekete,C.A., Mitchell,S.F., Cherkasova,V.A., Applefield,D., Algire,M.A., Maag,D., Saini,A., Lorsch,J.R. and Hinnebusch,A.G. (2007) N-and C-terminal residues of eIF1A have opposing effects on the fidelity of start codon selection. *EMBO* **26**, 1602–1614.
9. Cheung,Y.N., Maag,D., Mitchell,S.F., Fekete,C.A., Algire,M.A., Takacs,J.E., Shirokikh,N., Pestova,T., Lorsch,J.R. and Hinnebusch,A.G. (2007) Dissociation of eIF1 from the 40S ribosomal subunit is a key step in start codon selection in vivo. *Genes Dev.*, **21**, 1217–1230.
10. Saini,A.K., Nanda,J.S., Lorsch,J.R. and Hinnebusch,A.G. (2010) Regulatory elements in eIF1A control the fidelity of start codon selection by modulating tRNA(i)(Met) binding to the ribosome. *Genes Dev.*, **24**, 97–110.
11. Rabl,J., Leibundgut,M., Ataide,S.F., Haag,A. and Ban,N. (2011) Crystal structure of the eukaryotic 40S ribosomal subunit in complex with initiation factor 1. *Science*, **331**, 730–736.
12. Weisser,M., Voigts-Hoffmann,F., Rabl,J., Leibundgut,M. and Ban,N. (2013) The crystal structure of the eukaryotic 40S ribosomal subunit in complex with eIF1 and eIF1A. *Nat. Struct. Mol. Biol.*, **20**, 1015–1017.
13. Lomakin,I.B. and Steitz,T.A. (2013) The initiation of mammalian protein synthesis and mRNA scanning mechanism. *Nature*, **500**, 307–311.
14. Hussain,T., Llácer,J.L., Fernández,I.S., Munoz,A., Martin-Marcos,P., Savva,C.G., Lorsch,J.R., Hinnebusch,A.G. and Ramakrishnan,V. (2014) Structure of a eukaryotic translational initiation complex reveals key interactions in recognition of the start codon. *Cell*, **159**, 597–607.
15. Yu,Y., Marintchev,A., Kolupaeva,V.G., Unbehaun,A., Veryasova,T., Lai,S.C., Hong,P., Wagner,G., Hellen,C.U. and Pestova,T.V. (2009) Position of eukaryotic translation initiation factor eIF1A on the 40S ribosomal subunit mapped by directed hydroxyl radical probing. *Nucleic Acids Res.*, **37**, 5167–5182.
16. Yoon,H.J. and Donahue,T.F. (1992) The *sui1* suppressor locus in *Saccharomyces cerevisiae* encodes a translation factor that functions during $tRNA_i^{Met}$ recognition of the start codon. *Mol. Cell. Biol.*, **12**, 248–260.
17. Donahue,T. (2000) In: Sonenberg,N., Hershey,J.W.B. and Mathews,M.B. (eds), *Translational Control of Gene Expression*. Cold Spring Harbor Laboratory Press, Cold Spring Harbor, pp. 487–502.
18. Olsen,D.S., S,E.M., Mathew,A., Zhang,F., Krishnamoorthy,T., Phan,L. and Hinnebusch,A.G. (2003) Domains of eIF1A that mediate binding to eIF2, eIF3 and eIF5B and promote ternary complex recruitment *in vivo*. *EMBO J.*, **22**, 193–204.
19. Acker,M.G., Shin,B.S., Nanda,J.S., Saini,A.K., Dever,T.E. and Lorsch,J.R. (2009) Kinetic analysis of late steps of eukaryotic translation initiation. *J. Mol. Biol.*, **385**, 491–506.
20. Gietz,R.D. and Sugino,A. (1988) New yeast-Escherichia coli shuttle vectors constructed with in vitro mutagenized yeast genes lacking six-base pair restriction sites. *Gene*, **74**, 527–534.
21. Fekete,C.A., Applefield,D.J., Blakely,S.A., Shirokikh,N., Pestova,T., Lorsch,J.R. and Hinnebusch,A.G. (2005) The eIF1A C-terminal domain promotes initiation complex assembly, scanning and AUG selection in vivo. *EMBO J.*, **24**, 3588–3601.
22. Acker,M.G., Kolitz,S.E., Mitchell,S.F., Nanda,J.S. and Lorsch,J.R. (2007) Reconstitution of yeast translation initiation. *Methods Enzymol.*, **430**, 111–145.
23. Shin,B.S., Kim,J.R., Walker,S.E., Dong,J., Lorsch,J.R. and Dever,T.E. (2011) Initiation factor eIF2 promotes eIF2-GTP-Met-tRNA(i)(Met) ternary complex binding to the 40S ribosome. *Nat. Struct. Mol. Biol.*, **18**, 1227–1234.
24. Algire,M.A., Maag,D., Savio,P., Acker,M.G., Tarun,S.Z. Jr, Sachs,A.B., Asano,K., Nielsen,K.H., Olsen,D.S., Phan,L. *et al.* (2002) Development and characterization of a reconstituted yeast translation initiation system. *RNA*, **8**, 382–397.
25. Walker,S.E., Zhou,F., Mitchell,S.F., Larson,V.S., Valasek,L., Hinnebusch,A.G. and Lorsch,J.R. (2013) Yeast eIF4B binds to the head of the 40S ribosomal subunit and promotes mRNA recruitment through its N-terminal and internal repeat domains. *RNA*, **19**, 191–207.
26. Boeke,J.D., Trueheart,J., Natsoulis,G. and Fink,G.R. (1987) 5-fluoroorotic acid as a selective agent in yeast molecular genetics. *Methods Enzymol.*, **154**, 164–175.
27. Kapp,L.D., Kolitz,S.E. and Lorsch,J.R. (2006) Yeast initiator tRNA identity elements cooperate to influence multiple steps of translation initiation. *RNA*, **12**, 751–764.
28. Kolitz,S.E., Takacs,J.E. and Lorsch,J.R. (2009) Kinetic and thermodynamic analysis of the role of start codon/anticodon base pairing during eukaryotic translation initiation. *RNA*, **15**, 138–152.
29. Dong,J., Munoz,A., Kolitz,S.E., Saini,A.K., Chiu,W.L., Rahman,H., Lorsch,J.R. and Hinnebusch,A.G. (2014) Conserved residues in yeast initiator tRNA calibrate initiation accuracy by regulating preinitiation complex stability at the start codon. *Genes Dev.*, **28**, 502–520.
30. Dong,J., Nanda,J.S., Rahman,H., Pruitt,M.R., Shin,B.S., Wong,C.M., Lorsch,J.R. and Hinnebusch,A.G. (2008) Genetic identification of yeast 18S rRNA residues required for efficient recruitment of initiator tRNA(Met) and AUG selection. *Genes Dev.*, **22**, 2242–2255.
31. Dong,J., Qiu,H., Garcia-Barrio,M., Anderson,J. and Hinnebusch,A.G. (2000) Uncharged tRNA activates GCN2 by displacing the protein kinase moiety from a bipartite tRNA-binding domain. *Mol. Cell*, **6**, 269–279.
32. Hashem,Y., des Georges,A., Dhote,V., Langlois,R., Liao,H.Y., Grassucci,R.A., Hellen,C.U., Pestova,T.V. and Frank,J. (2013) Structure of the Mammalian Ribosomal 43S Preinitiation Complex Bound to the Scanning Factor DHX29. *Cell*, **153**, 1108–1119.
33. Hinnebusch,A.G. and Lorsch,J.R. (2012) The mechanism of eukaryotic translation initiation: new insights and challenges. *Cold Spring Harb. Perspect. Biol.*, **4**, 1–25.
34. Battiste,J.B., Pestova,T.V., Hellen,C.U.T. and Wagner,G. (2000) The eIF1A solution structure reveals a large RNA-binding surface important for scanning function. *Mol. Cell*, **5**, 109–119.
35. DeLano,W.L. (2002) PyMol Molecular Graphics System User's Manual. In: *PyMol User's Manual*. DeLano Scientific, Palo Alto, CA.
36. Taylor,D.J., Devkota,B., Huang,A.D., Topf,M., Narayanan,E., Sali,A., Harvey,S.C. and Frank,J. (2009) Comprehensive molecular structure of the eukaryotic ribosome. *Structure*, **17**, 1591–1604.